JOURNAL OF PETROLOGY | VOLUME 37 | NUMBER 5 | PAGES 999–1024 | 1996

ALBERTO E. PATIÑO DOUCE[1]* AND JAMES S. BEARD[2]
[1]DEPARTMENT OF GEOLOGY, UNIVERSITY OF GEORGIA, ATHENS, GA 30602, USA
[2]VIRGINIA MUSEUM OF NATURAL HISTORY, MARTINSVILLE, VA 24112, USA

Effects of P, $f(O_2)$ and Mg/Fe Ratio on Dehydration Melting of Model Metagreywackes

*We present results of dehydration melting experiments [3–15 kbar, 810–950°C, f(O_2) ≤ QFM (quartz–fayalite–magnetite) and ≥ Ni–NiO] on two Fe-rich mixtures of biotite (37%), plagioclase An_{38} (27%), quartz (34%) and ilmenite (2%), which differ only in their biotite compositions (*mg*-number 23 and 0·4). Dehydration melting of metagreywackes of constant modal composition generates a wide range of melt fractions, melt compositions and residual assemblages, through the combined effects of pressure, Fe/Mg ratio and f(O_2). Crystallization of garnet is the chief control on melting behavior, and is limited by two reactions: (1) the breakdown of garnet + quartz to orthopyroxene + plagioclase at low P, and (2) the oxidation of garnet to magnetite + anorthite + quartz (± enstatite), which is sensitive to both f(O_2) and P. Because of these reactions, melting of Mg-rich metagreywackes is rather insensitive to f(O_2) but strongly sensitive to P; the converse is true for Fe-rich metagreywackes. Garnet crystallization requires that plagioclase break down incongruently, liberating albite. This increases the Na_2O content of the melts and enhances melt production. Thus, melting of metagreywacke in a reducing deep-crustal environment (with garnet stable) would produce more, and more sodic, melt than would garnet-absent melting of the same source material in a relatively oxidizing, shallow-crustal environment.*

KEY WORDS: *anatexis; metasediments; gneisses; granites; garnet*

INTRODUCTION

Experimental studies with natural starting materials have shown that granitic melts can be produced by dehydration melting of biotite-bearing quartzofeldspathic metamorphic rocks (Le Breton & Thompson, 1988; Rutter & Wyllie, 1988; Vielzeuf & Holloway, 1988; Patiño Douce & Johnston, 1991; Skjerlie & Johnston, 1993; Vielzeuf & Montel, 1994; Patiño Douce & Beard, 1995; Gardien *et al.*, 1995; Dooley & Patiño Douce, 1996). Many of these studies have focused on determining the melting behavior of specific rocks, but some general conclusions about crustal anatexis have nevertheless emerged. For example, we now know that, given protoliths of comparable Fe/Mg ratios and TiO_2 and F contents, the fluid-absent solidus of metapelites is lower than that of less aluminous rocks by at least 100°C (e.g. Vielzeuf & Montel, 1994). Metagreywackes, however, produce greater volumes of granitic melts than metapelites, owing to their higher Na_2O contents (Patiño Douce & Johnston, 1991; Thompson, 1996). We also have evidence suggesting that melt production from the same protolith can remain approximately constant, or even increase, with increasing pressure, owing to the opposing effects of P on plagioclase stability and H_2O solubility (Patiño Douce, 1995; Patiño Douce & Beard, 1995).

The effect of Fe/Mg ratio on fluid-absent melting of biotite gneisses has received comparatively little attention, even though it is clear that metamorphic protoliths vary widely in their Fe/Mg ratios, and that this variation can have important consequences for the melting behavior of crustal rocks. Thus, whether garnet or orthopyroxene crystallizes as the dominant residual phase during melting of metagreywackes is strongly controlled by Fe/Mg ratio and by pressure (e.g. Patiño Douce, 1992). This mineralogical change can in turn affect the major and trace element compositions of the coexisting melt, and the melt fraction. The vapor-absent solidus temperatures of crustal rocks, and the sensitivity of mineral–melt equilibria to the prevailing

*Corresponding author. Telephone: 706-542-2394; fax: 706-542-2425; e-mail: alpatino@uga.cc.uga.edu

oxygen fugacity in the crust, are also likely to be affected by the Fe/Mg ratio. To address these issues we have studied the effects of Fe/Mg ratio, pressure and $f(O_2)$ on the fluid-absent melting relations of biotite-bearing rocks. This study demonstrates how interactions among these variables control melt fractions and melt and restite compositions during melting of metagreywackes, and leads to a more comprehensive understanding of crustal anatexis.

We report results of dehydration melting experiments with two simplified Fe-rich starting materials: a synthetic magnesian-annite gneiss (SMAG) and a synthetic F-annite gneiss (SFAG). Both consist of mixtures of hand-picked biotite, plagioclase, quartz and ilmenite. Their modal compositions are the same as that of the more magnesian synthetic biotite gneiss (SBG) studied by Patiño Douce & Beard (1995). Plagioclase, quartz and ilmenite used in the new starting materials are also the same minerals as used in SBG. The only difference among the starting materials is in the biotite composition, which varies from *mg*-number 55 in SBG to *mg*-number 23 in SMAG and *mg*-number 0·4 in SFAG [*mg*-number = 100 × Mg/(Mg + Fe), molar proportions]. Experiments were run at $P = 3$, 5, 7, 10 and 15 kbar, and at T from 840 to 950°C, covering most of the P–T range in which fluid-absent melting is likely to occur in the continental crust. The effect of $f(O_2)$ was evaluated by comparing experimental results from internally heated pressure vessel (IHPV), at $f(O_2) \geqslant$ Ni–NiO, with results from piston-cylinder apparatus (PC), at $f(O_2) \leqslant$ QFM (quartz–fayalite–magnetite). This experimental design allowed us to isolate the effects of Fe/Mg ratio, P, T and $f(O_2)$ from those of other compositional variables.

STARTING MATERIALS

The compositions of the synthetic starting materials (Table 1) were chosen so that the hydrous minerals were the phases that limited near-solidus melt production, but also so that they produced close to the maximum expected amount of granitoid melt by dehydration melting (Clemens & Vielzeuf, 1987). The procedure used to estimate these bulk compositions has been explained by Patiño Douce & Beard (1995). Enough ilmenite was added to saturate the experimental products in either ilmenite or rutile (at high P), so as to ensure that our results were not affected by the influence of TiO_2 on the stability of biotite (e.g. Ramberg, 1948; Robert, 1976; Dymek, 1983; Trønnes *et al.*, 1985; Patiño Douce, 1993).

Two large (> 5 cm) crystals of biotite (*mg*-numbers 0·4 and 23) were obtained from the mineralogy collection at the University of Georgia. The near end-member annite (*mg*-number 0·4) used in SFAG contains 1·9 wt % F (but no detectable Cl). This feature allowed us to investigate the effect of F on the stability of Fe-rich biotite (e.g. Munoz, 1984), and the controversial effect of F on the composition of melts derived from fluid-absent melting of

Table 1: Starting materials

	Modes[1]	SiO_2	Al_2O_3	TiO_2	FeO*[2]	MgO	MnO	CaO	Na_2O	K_2O	F	H_2O[3]	*mg*-no.[4]
Mineral compositions (wt %)[5]													
Biotite (SFAG)	37·2	33·3	13·5	1·0	36·7	0·1	1·0	0·3	0·2	8·3	1·9	2·6	0·4
Biotite (SMAG)	37·2	33·6	13·2	4·6	28·9	4·9	0·4	0·1	0·2	9·1	0·1	3·7	23·0
Plagioclase	26·5	58·7	26·2	—	—	—	—	7·9	7·1	0·1	—	—	—
Quartz	34·3	100·0	—	—	—	—	—	—	—	—	—	—	—
Ilmenite	2·0	0·0	0·0	52·7	45·4	0·5	1·3	0·0	—	—	—	—	2·0
Bulk compositions (wt %)[6]													
SFAG		62·2	12·0	1·4	14·6	0·04	0·4	2·2	2·0	3·1	0·7	1·0	0·5
SMAG		62·3	11·9	2·8	11·7	1·84	0·2	2·1	2·0	3·4	0·03	1·4	22·0

[1] Proportions by weight; both starting materials have the same mode.
[2] Total Fe as FeO.
[3] H_2O contents in micas estimated from stoichiometry, assuming (OH + F) = 2 per formula unit (12 oxygens). Bulk H_2O contents of starting materials estimated from H_2O contents in micas and modal compositions.
[4] *mg*-no. = MgO/(MgO + FeO*), molar proportions.
[5] Mineral compositions are averages of eight spot analyses (micas and plagioclase) and five spot analyses (ilmenite). Analytical uncertainties for all elements are always smaller than the corresponding uncertainties in minerals in the run products (see footnotes to Tables 5, 8 and 10).
[6] Calculated from mineral compositions and modal compositions.

halogen-enriched sources (see Dooley & Patiño Douce, 1996). Plagioclase (An_{38}) and quartz were also obtained from large (> 10 cm) individual crystals from the mineralogy collection at the University of Georgia, and ilmenite was obtained from a large crystal at the Virginia Museum of Natural History.

All minerals were ground to < 10 μm and mixed under acetone in an agate mortar. The powdered starting materials were stored in an oven at 130°C, and the loaded capsules were also kept in the oven for at least 24 h before welding. The bulk compositions of SFAG and SMAG were calculated from mineral analyses and modal composition (Table 1).

EXPERIMENTAL AND ANALYTICAL PROCEDURES

Experimental apparatus and sample containment

Experimental conditions and phase assemblages of experimental products are shown in Table 2. All experiments at $P \geqslant 7$ kbar, and one experiment at $P = 5$ kbar, were done in solid-medium piston-cylinder apparatus (PC) at the University of Georgia, with 0·5 in. diameter NaCl–graphite cell assemblies. Duration of most experiments was 2 weeks (Table 2). Temperatures were measured and controlled with W_{74}–Re_{26}/W_{95}–Re_5 thermocouples relative to electronic ice points (0°C) feeding Eurotherm 808 temperature controllers. Temperature stability during all runs was ±5°C. Use of small capsules resulted in the entire sample volume being within 2 mm of the thermocouple. This fact, and the consistent changes in modes and mineral compositions among experiments run at intervals of 25°C, suggest that temperature accuracy is on the order of 10°C. Samples were pressurized at room T to ~2 kbar below target P, heated to target T, and P finally released to target (hot, piston out). The pressures reported are Heise gauge oil pressures multiplied by ratio of ram-to-piston areas, and were manually maintained within ±0·2 kbar of target P. Friction loss in the cells is < 0·5 kbar, calibrated against the end-member breakdown reactions of anorthite and albite, and confirmed by mineral phase equilibria in run products at pressures of 5–15 kbar (Patiño Douce, 1995). On quenching, T dropped below 600°C in < 3 s. Samples in PC experiments were contained in welded Au capsules, 10 mm inner diameter with 0·2 mm wall, containing ~3 mg of sample. Capsules were paired side by side within the cells, so that each experiment contained one capsule of each bulk composition.

All 3 kbar and most 5 kbar experiments were performed at the Johnson Space Center in internally heated pressure vessels (IHPV). Capsules (2·7 mm inner diameter, 0·15 mm wall) and sample masses (~10 mg) were larger than in PC experiments, but other sample preparation techniques were similar. Pressures (argon pressure medium) were monitored by direct readings of calibrated Heise gauges. Uncertainty is ±0·1 kbar. Type-S (Pt:Pt10%Rh) thermocouples calibrated against the melting temperature of gold were used to measure T. Estimated T uncertainty is ±5°C. Run times were 7 days for experiments at 950°C and 14 days for all others (Table 2). Quench times to solidus T (850°C) were 10–30 s, and runs cooled to 600°C within 70 s. Quench crystallization was not observed.

All experiments were performed at $T \leqslant 950$°C. At these conditions, H_2O loss from gold capsules is not likely to be a severe problem (Patiño Douce & Beard, 1994), and we have not detected changes in phase relationships among experimental products that would indicate significant H_2O loss.

Oxygen fugacity

Oxygen fugacity was estimated for all experimental products that contained orthopyroxene and ilmenite from the equilibrium

$$2FeSiO_3 + \frac{1}{2}O_2 \rightleftharpoons Fe_2O_3 + 2SiO_2$$

using standard state properties from Berman (1988) and solution properties for orthopyroxene from Sack & Ghiorso (1989) and for ilmenite from Ghiorso (1990). In experiments that contained biotite and ilmenite, $f(O_2)$ was also estimated from the equilibrium

$$FeTiO_3 + \frac{3}{4}O_2 \rightleftharpoons [TiFe_{-2}]_{bio} + \frac{3}{2}Fe_2O_3$$

using the empirical calibration of Patiño Douce (1993). Oxygen fugacities estimated with both equilibria (Table 2) are in good agreement over about four orders of magnitude $f(O_2)$.

PC experiments lie between QFM and QFM − 2, whereas IHPV experiments generally lie above Ni–NiO, up to approximately QFM + 2. This shows that each experimental device generates redox conditions within a well-defined range, in complete agreement with the results of Patiño Douce & Beard (1995). External buffering of redox conditions is a consequence of the permeability of Au to H_2 and, perhaps, to volatile species with larger molecules too (Patiño Douce & Beard, 1994). The masses of the graphite furnace in the PC, and of the steel pressure

Table 2: Run conditions and phase assemblages

Run no.[1]	Duration (days)	P (kbar)	T (°C)	log $f(O_2)$ ΔQFM[2]	Assemblage[3]								
Synthetic F-annite gneiss (SFAG)													
1093-3/IH	14	3	840		Qtz	Pl					Ilm	Mag	Melt
1093-13/IH	14	3	875		Qtz	Pl					Ilm	Mag	Melt
1093-18/IH	14	3	900		Qtz	Pl					Ilm	Mag	Melt
1093-8/IH	14	3	925		Qtz	Pl					Ilm	Mag	Melt
1093-35/IH	14	5	840	−0·68	Qtz	Pl		Bt			Ilm	Mag	Melt
APD-543/PC	14	5	850		Qtz	Pl		Bt		Grt		Mag	Melt
293-3/IH	14	5	875		Qtz	Pl					Ilm	Mag	Melt
292-40/IH	14	5	900		Qtz	Pl					Ilm	Mag	Melt
1093-27/IH	14	5	925		Qtz	Pl					Ilm	Mag	Melt
293-9/IH	7	5	950		Qtz	Pl						Mag	Melt
APD-593/PC	16	7	810		Qtz	Pl		Bt	Amp	Grt	Ilm		
APD-532/PC	16	7	850	−3·01	Qtz	Pl		Bt		Grt	Ilm		Melt
APD-580/PC	14	7	875	−1·19	Qtz	Pl		Bt		Grt	Ilm		Melt
APD-530/PC	14	7	900		Qtz					Grt	Ilm		Melt
APD-594/PC	15	10	810		Qtz	Pl		Bt	Amp	Grt	Ilm		
APD-517/PC	16	10	850	−1·86	Qtz	Pl		Bt		Grt	Ilm		Melt
APD-512/PC	14	10	900	−1·13	Qtz	Pl	Kfs	Bt		Grt	Ilm		Melt
APD-581/PC	13	10	925		Qtz					Grt	Ilm		Melt
APD-514/PC	15	10	950	−0·75	Qtz			Bt		Grt	Ilm		Melt
APD-595/PC	14	15	860		Qtz	Pl		Bt		Grt	Ilm		
APD-537/PC	14	15	900	−1·11	Qtz		Kfs	Bt		Grt	Ilm		Melt
APD-579/PC	9	15	950	−0·78	Qtz			Bt		Grt	Ilm		Melt

Synthetic Mg-annite gneiss (SMAG)

1093-4/IH	14	3	840	1·62	Qtz	Pl		Bt				Ilm		Mag		Melt
1093-14/IH	14	3	875	1·44	Qtz	Pl					Opx	Ilm		Mag		Melt
1093-19/IH	14	3	900	1·69	Qtz	Pl					Opx	Ilm		Mag	Spl	Melt
1093-9/IH	14	3	925	1·67	Qtz	Pl					Opx	Ilm		Mag	Spl	Melt
1093-36/IH	14	5	840	1·10	Qtz	Pl		Bt				Ilm		Mag		Melt
APD-543/PC	14	5	850	−0·92	Qtz	Pl		Bt		Grt	Opx	Ilm				Melt
293-4/IH	14	5	875	1·19	Qtz	Pl		Bt			Opx	Ilm		Mag		Melt
292-45/IH	14	5	900	1·34	Qtz	Pl					Opx	Ilm		Mag		Melt
1093-28/IH	14	5	925	1·20	Qtz	Pl					Opx	Ilm		Mag	Spl	Melt
293-12/IH	7	5	950		Qtz	Pl					Opx	Ilm		Mag		Melt
APD-593/PC	16	7	810		Qtz	Pl		Bt	Amp	Grt		Ilm				
APD-532/PC	16	7	850	−1·56	Qtz	Pl		Bt		Grt	Opx	Ilm				Melt
APD-580/PC	14	7	875	−1·41	Qtz	Pl		Bt		Grt	Opx	Ilm				Melt
APD-530/PC	14	7	900	−1·83	Qtz	Pl				Grt	Opx	Ilm				Melt
APD-594/PC	15	10	810		Qtz	Pl		Bt		Grt		Ilm				Melt
APD-517/PC	16	10	850	−1·01	Qtz	Pl		Bt		Grt		Ilm				Melt
APD-512/PC	14	10	900	−0·87	Qtz	Pl		Bt		Grt		Ilm				Melt
APD-581/PC	13	10	925	−1·22	Qtz	Pl				Grt	Opx	Ilm				Melt
APD-514/PC	15	10	950	−1·37	Qtz	Pl	Kfs			Grt	Opx	Ilm				Melt
APD-595/PC	14	15	860		Qtz	Pl		Bt		Grt		Ilm				Melt
APD-537/PC	14	15	900	−0·25	Qtz	Pl	Kfs	Bt		Grt		Ilm				Melt
APD-579/PC	9	15	950		Qtz					Grt			Rt			Melt

[1]IH: internally heated pressure vessel experiment; PC: piston-cylinder experiment.
[2]Log $f(O_2)$ relative to the QFM buffer at the same pressure and temperature, calculated from mineral compositions in run products (see text).
[3]Mineral abbreviations in the tables and in the text are after Kretz (1983), except Amp: amphibole.

vessel in the IHPV, are many orders of magnitude greater than the sample mass and hence they impose their redox conditions on the sample.

Analytical procedures

Electron probe micro-analyses were performed in the JEOL JXA 8600 microprobe at the University of Georgia, using an accelerating voltage of 15 kV and sample current of 5 nA. To minimize alkali migration, and also to ensure accurate targeting, glass analyses were done in scanning mode at 50 000 × magnification, with the beam rastered over an area ~4 μm on a side. All other phases were also analyzed in scanning mode but with magnifications typically > 100 000 ×. Na and K were counted first, and Na was counted for 10 s. All other elements were counted for 40 s. Variations of K and Na count-rates with time at the analytical conditions for glass were investigated in several synthetic hydrous alkali-aluminosilicate glasses with H_2O contents comparable to those of the experimental glasses (2–5 wt %). Extrapolation of Na count-rate decay in the synthetic glasses resulted in a correction factor of 20% which was applied to the Na_2O values reported in Table 3. No count-rate decay was observed for K.

Modal compositions (Table 4) were calculated by simultaneous mass balance of K_2O, TiO_2, Al_2O_3, SiO_2, MgO, CaO and FeO*. Relative modal abundances of melt and total mafic phases, obtained from back-scattered electron (BSE) images, were used as additional constraints in the mass balance calculations [see also Patiño Douce & Johnston (1991)]. Uncertainties in the modal abundances of melt, quartz, plagioclase and ferromagnesian silicates are estimated to be less than ±4 wt %. Uncertainties in oxide modal abundances are estimated to be less than ±1 wt %. These estimates were obtained by carrying out replicate mass balance calculations, allowing phase compositions to vary within their analytical uncertainty ranges.

Approach to equilibrium

Patiño Douce & Beard (1995) demonstrated with crystallization experiments that dehydration melting experiments at $T \sim 900°C$ can achieve a reasonable approach to equilibrium in runs of ~2 weeks duration. Given that temperatures, melt fractions and run durations in these new experiments are similar to those of Patiño Douce & Beard (1995), our previous results suggest that a good approach to equilibrium was attained in this case too. Additionally, there are several consistent compositional trends among crystalline phases that suggest a good approach to equilibrium (see next section), and modal proportions of the experimental products also vary regularly with temperature and pressure (Table 4, Fig. 1).

MINERAL COMPOSITIONS AND STABILITY RELATIONSHIPS

Plagioclase

Plagioclase is a restite phase in most experiments (Table 5). It is absent only from high-temperature experiments at 10 kbar (SFAG) and 15 kbar (SFAG and SMAG). Plagioclase compositions in many charges are variable, with relict compositions preserved in the cores of larger grains, especially at low temperature. Plagioclase in experiments where there has been extensive melting is largely neoblastic, but zoning is evident even in some neoblasts. In general, neoblastic rims are well developed at low pressure ($\leqslant 7$ kbar), whereas unzoned neoblastic crystals predominate at higher pressures. Compositional trends are best developed among plagioclase neoblasts and rims that have the highest orthoclase content, suggesting plagioclase–melt equilibration during melting. Plagioclase becomes increasingly sodic as pressure increases owing to grossular-forming reactions that consume anorthite. However, plagioclase also tends to become more calcic as temperature and melt fraction increase (Table 5).

Alkali feldspar

Neoblastic alkali feldspar (Or_{59-70}; $An_{1\cdot6-3\cdot4}$; Table 5) occurs as a minor phase in a few melting experiments at $P \geqslant 10$ kbar. It is easily distinguished from plagioclase in BSE images, and it is unlikely that its presence in an experimental charge will go unnoticed. There is no observable change in the Or content of plagioclase related to whether or not alkali feldspar is present in the charge.

Crystallization experiments on SBG (Patiño Douce & Beard, 1995) suggest that alkali feldspar stability extends to $P < 10$ kbar. Its absence in low-P melting experiments may arise from nucleation difficulties related to the limited temperature range of stable coexistence of alkali feldspar plus melt at low P (Vielzeuf & Clemens, 1992) combined with overstepping of the dehydration melting reaction boundary. Increasing H_2O solubility with pressure lowers the K_2O/H_2O ratio of the melt and expands the stability field of alkali feldspar plus melt (Carrington & Watt, 1995; Patiño Douce & Beard, 1995), making crystallization of alkali feldspar in melting experiments more likely with increasing pressure.

Table 3: Glass compositions[1] (normalized to 100 wt % anhydrous)

P (kbar)	*T* (°C)	SiO_2	TiO_2	Al_2O_3	FeO*[2]	MnO	MgO	CaO	Na_2O[3]	K_2O	F	Total[4]	*mg*-no.[5]
Synthetic F-annite gneiss (SFAG)													
3	840	71·2	0·16	15·1	1·63	0·26	0·10	1·06	2·04	5·75	2·63	98·5	9·6
3	875	72·8	0·12	14·2	2·11	0·26	0·09	0·88	2·01	6·06	1·45	100·2	7·2
3	900	73·1	0·19	13·9	2·01	0·16	0·10	0·94	2·06	6·02	1·50	99·9	8·1
3	925	73·3	0·36	13·8	1·92	0·20	0·10	0·93	1·98	5·85	1·50	100·4	8·2
5	840	70·6	0·16	15·7	1·79	0·19	0·07	1·48	1·92	5·17	2·91	98·5	6·5
5	850	71·8	0·12	14·3	2·68	0·07	0·03	1·34	2·81	5·61	1·23	97·9	2·2
5	875	69·6	0·18	15·1	1·97	0·21	0·08	1·13	2·81	6·43	2·48	98·8	7·0
5	900	70·9	0·23	14·4	2·09	0·23	0·08	1·06	2·85	6·37	1·79	99·7	6·4
5	925	72·2	0·20	14·3	2·64	0·24	0·11	1·31	2·04	5·64	1·40	100·1	7·3
5	950	71·9	0·30	14·7	2·92	0·28	0·11	1·48	2·59	5·71	n.d.	98·2	6·3
7	850	71·1	0·07	14·7	2·66	0·03	0·01	1·20	3·25	5·42	1·52	96·8	0·8
7	875	72·7	0·14	13·8	2·45	0·03	0·01	1·28	3·27	5·26	1·07	98·1	0·4
7	900	71·1	0·21	14·6	2·67	0·10	0·04	1·67	3·18	5·21	1·19	97·9	2·5
10	850	70·3	0·16	15·2	2·64	0·04	0·01	1·02	3·90	5·07	1·64	96·3	0·4
10	900	71·2	0·16	15·3	2·45	0·03	0·01	1·07	2·91	5·09	1·78	97·2	0·9
10	925	70·9	0·21	14·3	2·91	0·06	0·03	1·38	3·14	5·38	1·66	98·4	2·0
10	950	70·2	0·18	14·8	2·90	0·03	0·02	1·08	3·79	5·61	1·43	98·2	1·0
15	900	70·2	0·20	15·5	2·12	0·02	0·02	0·75	4·12	5·14	1·95	97·9	1·4
15	950	70·6	0·25	14·3	2·72	0·07	0·06	0·87	3·88	5·75	1·54	98·6	3·5
Synthetic Mg-annite gneiss (SMAG)													
3	840	76·6	0·30	14·5	1·55	0·14	0·31	1·32	1·70	3·41	0·14	98·7	26·3
3	875	76·6	0·33	13·4	1·87	0·14	0·45	0·92	1·63	4·42	0·24	98·0	30·0
3	900	75·4	0·36	13·6	1·65	0·10	0·44	1·04	1·90	5·17	0·27	97·6	32·4
3	925	76·1	0·39	13·6	1·56	0·13	0·55	0·73	1·94	4·84	0·17	97·7	38·6
5	840	76·7	0·41	14·4	1·50	0·11	0·56	0·83	1·38	4·09	0·04	96·5	39·9
5	850	74·8	0·22	13·9	2·12	0·05	0·21	1·09	2·40	5·09	0·13	97·0	15·0
5	875	76·3	0·28	13·9	1·54	0·07	0·39	0·90	1·85	4·56	0·20	98·5	30·9
5	900	74·6	0·37	14·3	1·89	0·11	0·54	1·12	2·06	4·72	0·20	97·5	33·8
5	925	75·1	0·39	14·0	2·26	0·06	0·56	1·05	1·67	4·73	0·19	97·4	30·8
5	950	73·8	0·47	14·3	2·34	0·12	0·64	1·35	2·41	4·56	n.d.	97·1	32·7
7	850	74·1	0·25	14·5	1·76	0·03	0·21	1·49	2·79	4·57	0·32	95·6	17·7
7	875	75·2	0·16	14·0	1·73	0·02	0·16	1·28	2·60	4·71	0·19	96·2	13·8
7	900	73·3	0·45	13·9	2·19	0·04	0·32	1·09	2·61	5·88	0·17	97·3	20·9
10	850	74·3	0·24	15·1	1·60	0·04	0·22	1·22	2·81	4·38	0·10	93·8	19·4
10	900	74·6	0·18	14·5	1·71	0·05	0·18	1·15	2·75	4·74	0·10	95·4	15·8
10	925	73·5	0·36	14·3	1·72	0·00	0·25	1·46	3·02	4·99	0·35	97·6	20·9
10	950	73·1	0·28	14·6	1·79	0·02	0·25	1·20	3·06	5·55	0·12	98·6	19·9
15	860	75·7	0·16	14·8	0·92	0·05	0·14	0·99	2·82	4·49	0·02	94·4	21·4
15	900	73·4	0·31	14·7	1·40	0·03	0·19	0·86	3·74	5·29	0·06	96·6	19·3
15	950	73·8	0·32	14·3	1·63	0·04	0·21	0·88	3·63	4·98	0·18	98·2	18·6

[1]Values are averages of four (in some near-solidus runs) to ten (in most runs) analyses of different glass pools. Typical relative uncertainties (2 S.D. of the mean values) are: SiO_2, ±1%; TiO_2, ±15%; Al_2O_3, ±3%; FeO*, ±8%; MnO, ±80%; MgO, ±15% (SMAG) ±50% (SFAG); CaO, ±10%; Na_2O, ±15%; K_2O, ±4%; F, ±12%.
[2]FeO*, total Fe given as FeO.
[3]Reported values include 20% correction factor for Na loss during probing (see text).
[4]Probe total (including 20% correction factor for Na_2O), minus F equivalent.
[5]*mg*-no. = 100 × MgO/(MgO + FeO*), molar proportions.

Table 4: Modal compositions (wt %)[1]

P (kbar)	*T* (°C)	App.[2]	Qtz	Pl	Kfs	Bt	Grt	Opx	Ilm[3]	Mag[4]	Melt
Synthetic F-annite gneiss (SFAG)											
3	840	IH	26	23	0	0	0	0	3	16	31
3	875	IH	26	23	0	0	0	0	2	17	31
3	900	IH	22	21	0	0	0	0	0	19	38
3	925	IH	22	20	0	0	0	0	2	16	39
5	840	IH	32	23	0	11	0	0	1	15	18
5	850	PC	21	14	0	8	15	0	0	8	35
5	875	IH	27	23	0	0	0	0	1	18	31
5	900	IH	26	21	0	0	0	0	1	18	34
5	925	IH	23	21	0	0	0	0	1	18	37
5	950	IH	25	19	0	0	0	0	0	18	37
7	850	PC	20	13	0	17	19	0	2	0	29
7	875	PC	17	4	0	15	23	0	2	0	40
7	900	PC	8	0	0	0	31	0	3	0	69
10	850	PC	22	11	0	20	19	0	1	0	26
10	900	PC	14	5	0	16	21	0	1	0	44
10	925	PC	9	0	0	0	33	0	2	0	56
10	950	PC	8	0	0	4	27	0	1	0	60
15	900	PC	27	0	14	8	31	0	2	0	18
15	950	PC	12	0	0	1	32	0	2	0	53
Synthetic Mg-annite gneiss (SMAG)											
3	875	IH	19	21	0	0	0	7	6	8	39
3	900	IH	18	19	0	0	0	6	8	7	41
3	925	IH	17	18	0	0	0	7	10	5	42
5	850	PC	24	18	0	4	11	12	5	0	26
5	875	IH	22	21	0	4	0	7	8	6	31
5	900	IH	22	19	0	0	0	7	7	7	37
5	925	IH	19	19	0	0	0	8	7	7	39
5	950	IH	22	19	0	0	0	6	7	8	37
7	850	PC	30	14	0	8	21	3	4	0	19
7	875	PC	19	12	0	1	18	8	5	0	37
7	900	PC	13	17	0	0	7	18	5	0	40
10	850	PC	31	10	0	11	24	0	4	0	20
10	900	PC	21	7	0	9	24	0	4	0	35
10	925	PC	15	1	0	0	29	1	4	0	50
10	950	PC	14	1	3	0	26	2	5	0	50
15	860	PC	34	23	0	26	6	0	4	0	8
15	900	PC	27	5	3	27	20	0	1	0	18
15	950	PC	16	0	0	0	38	0	2	0	44

[1]Modal compositions calculated by simultaneous mass-balance of SiO_2, Al_2O_3, TiO_2, MgO, FeO*, CaO and K_2O, constrained by point-counting of BSE images. Uncertainties in modal abundances are less than ± 4 wt % for most phases, except ± 1 wt % for oxides (see text).
[2]Experimental apparatus (IH, internally heated pressure vessel; PC, piston-cylinder).
[3]Rutile in SMAG at 15 kbar and 950°C.
[4]Magnetite + Al-spinel.

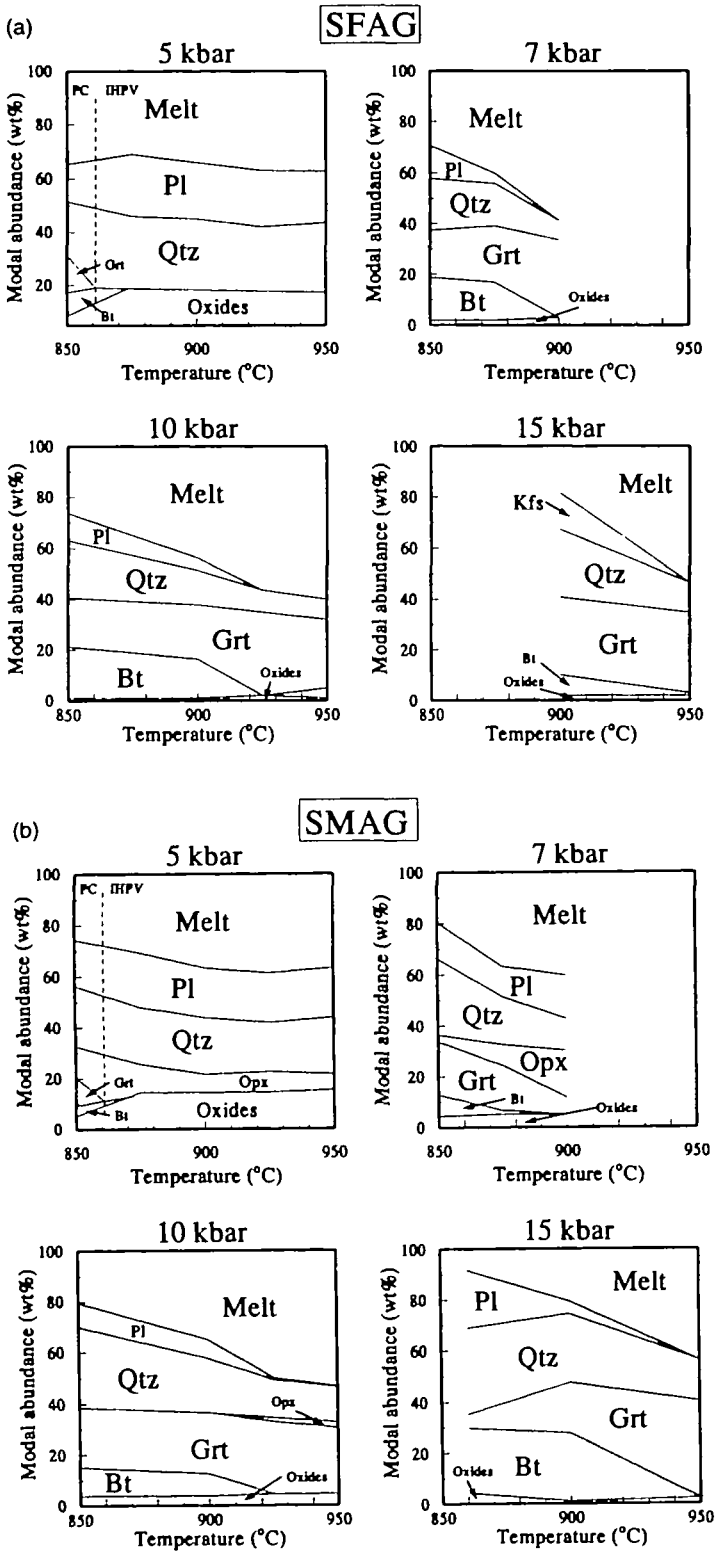

Fig. 1. Isobaric changes in modal compositions for synthetic F-annite gneiss (a) and for synthetic Mg-annite gneiss (b). Experiments at 5 kbar and $T > 850°C$ were in internally heated pressure vessel; experiment at 850°C and 5 kbar and all experiments at higher pressure were in piston-cylinder apparatus. Mineral abbreviations after Kretz (1983).

Table 5: Feldspar compositions (wt %)[1]

P (kbar)	*T* (°C)	SiO_2	Al_2O_3	FeO*[2]	CaO	Na_2O	K_2O	Total	An[3]	Ab	Or
Plagioclase—synthetic F-annite gneiss (SFAG)											
3	840	59·6	26·2	0·30	8·23	5·83	0·83	101·0	41	52	7
3	875	59·2	26·2	0·56	8·49	5·78	1·13	101·3	41	49	11
3	900	58·1	26·0	0·76	8·61	5·33	1·26	100·1	44	48	9
3	925	58·1	26·6	0·68	9·15	5·10	1·14	100·8	46	46	7
5	840	59·0	26·4	0·60	8·43	5·55	1·09	101·0	43	49	9
5	850	59·4	26·0	0·63	8·51	6·11	0·77	101·4	42	54	4
5	875	58·5	26·3	0·41	8·32	6·77	0·93	101·2	38	53	9
5	900	58·2	26·6	0·52	8·67	6·37	1·05	101·5	44	48	8
5	925	58·7	26·0	0·45	8·66	5·49	1·31	100·6	41	48	11
5	950	57·3	27·2	0·44	9·34	5·06	1·09	100·5	45	48	7
7	850	59·8	26·2	0·59	7·84	6·19	0·58	101·3	40	57	3
7	875	59·2	25·7	0·41	8·01	6·45	0·61	100·4	39	57	4
10	850	58·0	26·7	0·76	7·92	7·00	0·47	100·8	37	60	3
10	900	58·3	26·8	0·63	7·96	7·00	0·33	101·0	38	60	2
15	860	61·0	25·0	0·53	7·04	7·44	0·57	101·6	33	64	3
Neoblastic alkali feldspar—synthetic F-annite gneiss (SFAG)											
10	900	65·1	19·6	0·71	0·7	4·06	10·61	100·8	3	36	61
15	900	65·5	19·1	0·51	0·33	4·06	10·95	100·5	2	35	63
Plagioclase—synthetic Mg-annite gneiss (SMAG)											
3	840	58·8	26·2	0·48	8·40	5·53	0·94	100·4	43	50	6
3	875	58·6	26·4	0·43	8·85	6·63	1·03	101·9	41	53	6
3	900	58·2	26·1	0·61	8·73	5·09	1·12	99·8	48	42	9
3	925	58·3	26·7	0·45	9·18	4·90	0·92	100·4	46	47	7
5	840	59·0	26·5	0·64	8·34	5·92	0·74	101·2	42	52	6
5	850	58·5	26·2	0·54	8·81	5·45	0·51	100·1	46	51	3
5	875	58·4	26·6	0·61	8·53	6·86	0·91	101·9	39	56	6
5	900	57·6	26·4	0·58	8·96	6·30	1·08	100·9	42	51	7
5	925	58·4	26·3	0·57	8·78	5·47	0·88	100·5	45	49	6
5	950	55·8	27·2	0·52	9·57	4·97	0·79	98·9	43	52	6
7	850	58·2	26·5	0·45	8·17	6·36	0·42	100·1	40	57	2
7	875	58·8	26·0	0·29	8·35	6·57	0·36	100·4	40	58	2
7	900	58·4	26·8	0·45	8·43	5·80	1·11	101·0	42	52	7
10	850	57·5	26·6	0·48	7·93	7·14	0·49	100·1	37	60	3
10	900	59·1	26·7	0·41	7·97	7·01	0·45	101·7	38	60	3
10	925	58·3	26·5	0·29	8·11	6·15	0·43	99·7	41	56	3
10	950	57·2	26·5	0·39	8·07	6·47	0·96	99·5	39	56	5
15	900	58·5	26·7	0·44	7·90	6·29	0·29	100·1	40	58	2
Neoblastic alkali feldspar—synthetic Mg-annite gneiss (SMAG)											
10	950	62·4	19·4	0·49	0·55	3·08	11·72	97·7	3	28	70
15	900	64·6	19·5	0·6	0·59	4·21	10·04	99·6	3	38	59

[1]Wt % compositions are averages of four analyses of plagioclase rims and/or of small neoblastic crystals, except two analyses for alkali feldspar crystals. Typical relative uncertainties (2 S.D. of the mean values) are: SiO_2, ± 2%; Al_2O_3, ± 3%; FeO*, ± 15%; CaO, ± 5% (Pl) or ± 15% (Kfs); Na_2O, ± 10%; K_2O, ± 15% (Pl) or ± 2% (Kfs).
[2]FeO*, total Fe given as FeO.
[3]End-member compositions are for the most Or-rich spot analysis in each experimental charge.

Orthopyroxene

Orthopyroxene is present in supersolidus experiments with SMAG from 3 to 7 kbar at $T \geqslant 850°C$, and at $T \geqslant 925°C$ at 10 kbar. It is absent from experiments with SMAG at 15 kbar, and from all experiments with SFAG. The orthopyroxene is aluminous (in some cases extremely aluminous) hypersthene (Table 6). Al_2O_3 contents in opx formed in 3 and 5 kbar experiments on SMAG (both PC and IHPV) range from 6·0 to 10·9 wt %. At 7–10 kbar, Al_2O_3 content is lower, ranging from 3·0 to 6·4 wt %.

The most magnesian opx (En_{54-67}) occurs in the IHPV experiments (Table 6). The low *mg*-number of opx formed in the 5 kbar PC experiment (Table 6) suggests that the high *mg*-number of IHPV opx is caused by the elevated Fe^{3+} content in the more oxidized IHPV experiments. In both IHPV and PC experiments, opx generally becomes more magnesian as temperature and melt fraction increase (Table 6). Low-pressure opx is Ca poor in all 3–5 kbar PC and IHPV experiments. The Ca content of opx generally increases with pressure above 5 kbar (Table 6). In general, opx that coexists with garnet is more calcic than that which does not.

Amphibole

The only chain silicates found in experiments on the Fe-rich starting composition SFAG are sodic–calcic amphiboles (ferro-barroisite) that occur in the subsolidus (810°C) experiments at 7 and 10 kbar (Table 6). The presence of this unusual phase probably reflects the overall instability of extremely Fe-rich orthopyroxene (e.g. Bohlen *et al.*, 1980) and the reduced stabilities of hedenbergite and fayalite under relatively high water activity. Aluminous gedrite (16 wt % Al_2O_3) is found in the 7 kbar subsolidus (810°C) experiment on SMAG. It may have formed, together with garnet, by a reaction among biotite, plagioclase and ilmenite.

Garnet

The pressure stability of garnet is a function of

Table 6: Orthopyroxene and amphibole compositions (wt %)[1]

P (kbar)	*T* (°C)	SiO_2	TiO_2	Al_2O_3	FeO*[2]	MnO	MgO	CaO	Na_2O	K_2O	Total	*mg*-no.[3]
Amphibole—synthetic F-annite gneiss (SFAG)												
7	810	43·0	0·48	12·87	30·4	1·63	0·18	6·98	2·00	0·90	98·5	1·0
10	810	44·1	0·38	15·87	29·1	1·60	0·15	6·51	3·03	0·89	101·7	0·9
Orthopyroxene—synthetic Mg-annite gneiss (SMAG)												
3	875	49·0	0·49	8·50	20·1	0·84	19·93	0·19			99·1	63·9
3	900	49·3	0·41	10·49	18·5	0·88	21·06	0·58			101·2	66·9
3	925	51·2	0·72	10·89	19·9	0·80	18·09	0·29			101·8	61·8
5	850	46·4	0·49	8·29	35·3	0·53	8·50	0·28			99·8	30·0
5	875	52·6	0·48	9·04	22·1	0·74	14·67	0·26			99·9	54·1
5	900	48·2	0·40	9·93	21·1	0·80	18·73	0·23			99·4	61·2
5	925	50·1	0·54	6·02	20·7	0·76	20·29	0·39			98·8	63·4
5	950	45·4	0·57	10·17	19·6	0·79	21·23	0·24			98·0	65·9
7	850	47·8	0·21	5·19	34·4	0·31	10·61	0·43			99·0	35·5
7	875	48·1	0·28	4·72	34·3	0·30	11·52	0·52			99·8	37·4
7	900	48·3	0·26	3·01	34·5	0·19	12·52	0·48			99·3	39·3
10	925	49·9	0·43	3·36	28·4	0·08	15·50	0·94			98·5	49·3
10	950	48·1	0·36	6·41	29·6	0·20	13·98	0·71			99·4	45·7
Amphibole—synthetic Mg-annite gneiss (SMAG)												
7	810	41·8	0·76	16·07	31·6	0·68	5·74	0·86	1·45	0·01	98·9	24·5

[1]Values are averages of 5–6 analyses of different crystals (Opx) or 3–4 analyses of different crystals (Amp). Typical relative uncertainties (2 S.D. of the mean values) are: SiO_2, ± 2%; TiO_2, ± 15%; Al_2O_3, ± 5%; FeO*, ± 2%; MnO, ± 20%; MgO, ± 7%; CaO, ± 15%; Na_2O, ± 10%; K_2O, ± 25%.
[2]FeO*, total Fe given as FeO.
[3]*mg*-no. = 100 × MgO/(MgO + FeO*), molar proportions.

starting composition and oxygen fugacity. Garnet is stable at pressures of 5 kbar and above in PC experiments in both Fe-rich compositions SFAG and SMAG, but is not stable at $P < 12{\cdot}5$ kbar in SBG (see Patiño Douce & Beard, 1995). Garnet is not found in any IHPV experiment. Garnet compositions are given in Table 7. The Mg/Fe ratios of all garnets are primarily determined by the bulk composition (Table 7). For all bulk compositions, MnO and FeO tend to decrease and MgO tends to increase with increasing temperature and melt fraction (Table 7). In both SFAG and SMAG, garnet CaO contents in experiments containing plagioclase increase with pressure at a given melt fraction.

Garnets in the most Fe-rich composition (SFAG) are Fe–Ca–Mn garnets, with pyrope content averaging < 1 mol %. In experiments on SMAG, garnet coexists with opx at 5 and 7 kbar and at $T \geqslant 925$°C at 10 kbar. Garnets that coexist with opx are less calcic than the higher-P and/or lower-T garnets that do not.

Biotite

Biotite is present at all pressures investigated, except

Table 7: Garnet compositions (wt %)[1]

P (kbar)	T (°C)	SiO_2	TiO_2	Al_2O_3	FeO*[2]	MnO	MgO	CaO	Total	*mg*-no.[3]
Synthetic F-annite gneiss (SFAG)										
5	850	35·8	0·83	20·5	36·1	3·12	0·34	3·49	100·2	1·6
7	810	36·3	0·48	19·7	27·5	6·78	0·03	7·46	98·3	0·2
7	850	36·3	0·42	20·0	35·6	2·30	0·10	4·21	99·0	0·5
7	875	36·9	0·62	19·3	34·7	1·95	0·13	5·88	99·4	0·6
7	900	36·6	0·34	20·6	37·1	0·28	0·46	4·90	100·2	2·2
10	810	36·9	0·40	20·0	28·9	4·85	0·06	8·19	99·3	0·4
10	850	36·0	0·38	20·0	34·4	1·48	0·11	5·33	97·7	0·6
10	900	36·5	0·39	20·2	36·2	0 42	0·15	6·13	100·0	0·7
10	925	36·7	0·51	19·6	34·9	1·05	0·53	5·34	98·6	2·6
10	950	35·8	0·62	19·7	35·0	1·19	0·28	5·72	98·3	1·4
15	860	36·6	0·42	19·2	29·5	2·94	0·07	9·33	98·0	0·4
15	900	36·8	0·63	19·9	35·7	0·49	0·12	6·53	100·2	0·6
15	950	36·9	0·37	19·2	36·4	1·27	0·33	5·34	99·9	1·6
Synthetic Mg-annite gneiss (SMAG)										
5	850	37·2	0·73	21·1	33·7	0·92	3·94	2·46	100·0	17·2
7	810	36·6	1·13	20·1	34·3	2·10	2·34	3·13	99·8	10·8
7	850	36·5	0·92	20·2	33·2	1·14	3·45	3·40	98·8	15·6
7	875	37·2	0·95	19·4	32·6	0·93	3·78	3·76	98·7	17·1
7	900	37·9	0·77	20·2	33·6	0·62	5·32	2·70	101·1	22·0
10	810	37·2	0·72	20·4	33·2	1·02	2·77	4·04	99·2	13·0
10	850	36·5	1·17	20·7	31·8	0·76	3·38	4·93	99·2	15·9
10	900	37·1	1·07	20·6	31·9	0·66	3 68	4·78	99·8	17·1
10	925	37·3	1·33	20·5	29·9	0·46	4·88	4·72	99·1	22·5
10	950	36·7	1·11	20·6	30·7	0·77	4·54	4·17	98·5	20·9
15	860	37·5	0·89	19·5	31·7	0·64	3·52	5·12	98·9	16·5
15	900	37·3	1·52	20·2	30·2	0·83	3·39	6·35	99·9	16·7
15	950	37·9	1·11	19·6	28·6	0·49	3·90	7·41	99·0	19·6

[1]Values are averages of 5–6 analyses of different crystals, except three analyses in 850°C, 7 kbar runs. Typical relative uncertainties (2 S.D. of the mean values) are: SiO_2, ± 2%; TiO_2, ± 15%; Al_2O_3, ± 2%; FeO*, ± 2%; MnO, ± 15%; MgO, ± 7%; CaO, ± 5%.
[2]FeO*, total Fe given as FeO.
[3]*mg*-no.= 100 × MgO/(MgO + FeO*), molar proportions.

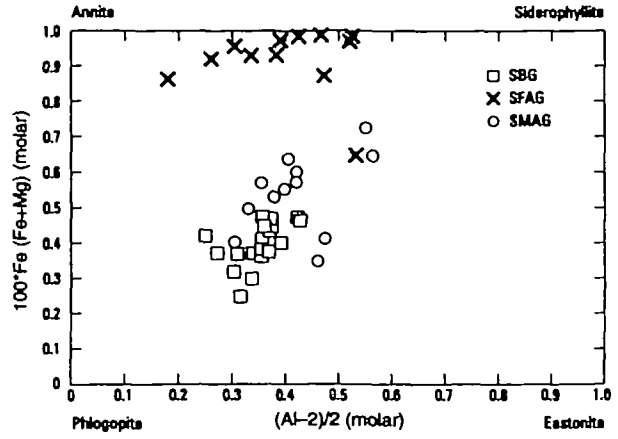

Fig. 2. Annite–eastonite diagram for biotite. SBG data from Patiño Douce & Beard (1995).

in SFAG at 3 kbar. The Mg/Fe ratio of biotite in the run products reflects Mg/Fe ratio in the starting materials, but within each bulk composition there is a considerable range in Mg/Fe ratios in biotite coexisting with melt (Fig. 2). As is the case for other mafic silicates, the *mg*-number of biotite in the relatively oxidized IHPV experiments is higher than that in the more reducing PC experiments. This contrast is especially strong in experiments with SFAG (Table 8). In PC experiments, biotite becomes more magnesian with increasing temperature and melt fraction. Within each bulk composition biotite tends to become more aluminous with decreasing Mg/Fe ratio (Fig. 2).

The F content in biotite (and melt) reflects the F content in the starting material, so that SFAG contains the most F-rich biotites (Table 8). There also appears to be a relationship between F content and $f(O_2)$, with the most F-rich biotites generally occurring in IHPV experiments, which are more oxidized than PC experiments (Table 8). The Ti content of biotite increases with temperature and melt fraction for all starting materials. Above the solidus, biotite Ti content at a given temperature or melt fraction tends to be highest at the highest pressures (Table 8).

Magnetite and spinel

Magnetite is a ubiquitous phase in IHPV experiments but is absent in all PC experiments except for the 5 kbar, 850°C experiment on SFAG. The magnetite in this experiment is the most TiO_2 rich of all experiments [Usp/(Usp + Mag) = 042; Table 9], consistent with the reducing conditions in the PC. Usp/(Usp + Mag) in IHPV experiments ranges from 0·08 to 0·31 and averages 0·18–0·23. The lowest TiO_2 magnetites occur at 840°C. A range of values is seen at other temperatures, but there is no clear correlation between T and Usp concentration above 840°C (Table 9). Magnetites are generally aluminous, with (Spl + Hc) component ranging from 11 to 19 mol % in SFAG, and from 22 to 28 mol % in SMAG. Mg and Al both generally increase with temperature (Table 9). Aluminous spinels coexist with magnetite in several experiments on SMAG (Table 9). These spinels occur both as separate grains and as intergrowths with magnetite.

Ilmenite and rutile

Ilmenite occurs in all experiments except for high-T experiments at 15 kbar, where it is replaced by rutile. Ilmenite in IHPV experiments is enriched in Fe_2O_3 and Al_2O_3 with respect to the more reducing PC experiments (Table 10). Mg is uniformly low in experiments on SFAG but increases with temperature in the more magnesian compositions.

PHASE RELATIONS AND MELTING REACTIONS

The solidus of the more Fe-rich composition (SFAG) has been bracketed at 7, 10, and 15 kbar (Fig. 3). Within this P range it has positive dP/dT slope, from $T = 810$–850°C at 7 kbar to $T = 860$–900°C at 15 kbar. The solidus of SMAG has only been bracketed at 7 kbar (Fig. 3), but its position can be inferred from curves of constant melt fraction (Fig. 4). The inferred SMAG solidus has negative to vertical dP/dT slope at $P \leqslant 10$ kbar, and positive slope between 10 and 15 kbar. The change in slope can be inferred on the basis of PC experiments only ($P \geqslant 7$ kbar), so that it is unlikely to be an artifact of the different oxidation conditions imposed by each experimental setup. At $P \geqslant 7$ kbar the solidus of SFAG is located at a higher T than that of SMAG (Fig. 3). This difference demonstrates that the strong stabilizing effect of F in micas, which has been well documented for phlogopite (e.g. Peterson *et al.*, 1991; Dooley & Patiño Douce, 1996), is also important for Fe-rich compositions. This conclusion is contrary to the suggestion of Munoz (1984) that F substitution decreases the thermal stability of annite.

It has often been inferred that dehydration melting solidi should bend back (from positive to negative dP/dT slope) with rising P, in response to crystallization of restitic garnet (e.g. Lambert & Wyllie, 1972; Burnham, 1979; Le Breton & Thompson, 1988; Rushmer, 1991; Wyllie & Wolf, 1993). This inferred behavior is not borne out by the melting relations of SFAG nor of SMAG, even though garnet is produced by the initial dehydration melting reactions of both Fe-rich compositions at

Table 8: Biotite compositions (wt %)[1]

P (kbar)	*T* (°C)	SiO_2	TiO_2	Al_2O_3	FeO*[2]	MnO	MgO	Na_2O	K_2O	F	Total[3]	*mg*-no.[4]
Synthetic F-annite gneiss (SFAG)												
5	840	37·8	2·37	16·9	21·0	0·97	6·47	0·35	8·82	5·90	98·1	35·4
5	850	37·1	3·18	16·1	30·0	0·15	2·43	0·53	8·40	2·62	99·4	12·6
7	810	33·5	3·04	15·7	32·8	0·88	0·28	0·63	8·26	2·09	96·3	1·5
7	850	33·4	2·59	15·7	34·6	0·10	0·59	0·43	8·31	2·50	97·2	3·0
7	875	34·3	4·88	13·5	32·9	0·08	0·85	0·39	8·72	1·94	96·7	4·4
10	810	33·9	3·62	15·2	33·2	0·45	0·23	0·34	8·48	1·97	96·6	1·2
10	850	36·5	3·91	14·8	31·7	0·03	0·51	0·65	8·31	2·16	97·7	2·8
10	900	34·1	5·15	14·5	31·7	0·03	1·27	0·52	8·68	2·41	97·4	6·7
10	950	34·9	5·76	13·3	31·3	0·09	1·52	0·50	8·62	2·05	97·1	8·0
15	860	37·5	2·52	15·3	31·9	0·18	0·30	0·65	8·44	2·21	98·1	1·6
15	900	35·7	5·51	14·2	30·1	0·06	1·27	0·53	8·85	2·06	97·4	7·0
15	950	36·3	6·18	12·5	28·7	0·12	2·53	0·37	8·80	2·09	96·7	13·6
Synthetic Mg-annite gneiss (SMAG)												
3	840	38·0	5·01	17·1	13·3	0·28	13·95	0·53	8·53	0·45	97·0	65·2
5	840	38·2	4·68	17·0	14·9	0·27	12·15	0·45	8·47	0·43	96·4	59·2
5	850	36·9	5·36	15·9	20·8	0·03	7·73	0·40	8·58	0·64	96·1	39·9
5	875	41·9	4·44	15·3	13·8	0·25	11·58	0·80	7·15	0·85	95·7	60·0
7	810	35·3	3·85	17·0	25·5	0·05	5·49	0·49	8·51	0·43	96·4	27·7
7	850	36·8	4·97	15·6	19·9	0·05	9·08	0·56	8·49	0·61	95·9	44·8
7	875	36·5	4·98	15·0	21·0	0·05	8·83	0·52	8·95	0·56	96·2	42·8
10	810	34·7	4·14	17·1	23·0	0·12	7·10	0·49	8·60	0·51	95·6	35·5
10	850	35·6	5·55	15·8	20·9	0·01	8·74	0·61	8·85	0·47	96·3	42·8
10	900	37·1	6·05	15·7	19·3	0·05	9·54	0·60	8·85	0·47	97·5	46·8
15	860	39·0	5·52	16·0	20·4	0·00	6·60	0·68	8·58	0·53	97·0	36·6
15	900	37·7	6·99	15·3	17·9	0·03	10·11	0·55	9·09	0·50	98·0	50·1

[1]Values are averages of 5–8 analyses of different crystals. Typical relative uncertainties (2 S.D. of the mean values) are: SiO_2, ± 2%; TiO_2, ± 4%; Al_2O_3, ± 3%; FeO*, ± 2%; MnO, ± 50%; MgO, ± 2%; Na_2O, ± 20%; K_2O, ± 5%; F, ± 10%.
[2]FeO*, total Fe given as FeO.
[3]Probe total minus F equivalent.
[4]*mg*-no. = 100 × MgO/(MgO + FeO*), molar proportions.

$f(O_2) \leqslant$ QFM and $P = 5$–15 kbar. We suggest that the proportions in which garnet crystallizes during the incongruent melting reactions are not sufficient to offset the much greater molar volume of the melt phase. Therefore, ΔV of the incongruent melting reaction remains positive, and the solidus does not bend back, at least at $P \leqslant 15$ kbar [see Patiño Douce & Beard (1995) for discussion of analogous behavior in more magnesian biotite-bearing protoliths].

The change in oxidation conditions, from $f(O_2) \geqslant$ Ni–NiO in IHPV experiments to $f(O_2) \leqslant$ QFM in PC experiments, causes changes in the dehydration melting reactions of SFAG and SMAG. These changes are strikingly demonstrated by the overlapping PC and IHPV experiments at 5 kbar (Fig. 3, Tables 2 and 4). Silicate mafic phases (Opx > Grt in SMAG, Grt only in SFAG) are the chief solid products of dehydration melting at 5 kbar and $f(O_2) \leqslant$ QFM (PC experiment). These phases are replaced by oxide phases (Mag ≫ Ilm in SFAG, Mag ≈ Ilm in SMAG) in the incongruent melting reaction at 5 kbar and $f(O_2) \geqslant$ Ni–NiO (IHPV experiments). Orthopyroxene crystallizes above the solidus ($T \geqslant$ 875°C) in IHPV experiments [$f(O_2) \geqslant$ Ni–NiO] with SMAG, but not in equivalent experiments with the more ferroan composition. Garnet is absent from all IHPV experimental products. Predictably, these results show that changes in $f(O_2)$ have a stronger effect on the residual assemblages produced from these Fe-rich compositions than on the residual

Table 9: Magnetite and spinel compositions (wt %)[1]

P (kbar)	*T* (°C)	SiO_2	TiO_2	Al_2O_3	FeO	Fe_2O_3[2]	MnO	MgO	Total
Magnetite—synthetic F-annite gneiss (SFAG)									
3	840	0·20	4·19	7·57	32·7	48·2	1·78	0·29	95·0
3	875	0·72	5·00	8·62	35·8	47·1	1·45	0·39	99·0
3	900	0·12	9·49	6·32	37·9	41·6	1·74	0·46	97·6
3	900	0·17	5·60	7·71	34·3	45·5	1·32	0·40	95·0
3	925	0·31	4·70	7·42	33·9	48·7	1·63	0·45	97·1
5	840	0·53	5 17	8·45	35·1	45·7	1·56	0·22	96·8
5	850	0·36	12·90	4·92	43·1	35·5	0·26	0·09	97·2
5	875	0·23	7·22	7·37	36·4	44·4	1·56	0·38	97·6
5	900	0·24	7·35	7·80	36·8	43·6	1·45	0·38	97·6
5	925	0·21	7·91	7·35	37·4	43·4	1·40	0·34	97·9
5	925	0·47	5·24	8·30	35·5	46·7	1·28	0·36	97·9
5	950	0·32	7·46	7·63	36·6	42·0	1·25	0·34	95·6
Magnetite—synthetic Mg-annite gneiss (SMAG)									
3	840	0·31	3·26	10·32	30·5	49·9	1·05	2·69	98·0
3	875	0·25	6·39	10·78	34·9	43·9	0·52	2·26	99·0
3	900	0·24	5·33	12·04	32·7	44·8	0·57	3·08	98·7
3	925	0·58	2·88	13·64	27·7	46·9	0·91	4·83	97·4
5	840	0·68	4·08	11·85	33·0	44·5	0·96	1·90	96·9
5	875	0·46	4·76	12·13	33·2	44·7	0·66	2·49	98·3
5	900	0·22	5·48	13·28	33·3	42·7	0·65	2·79	98·4
5	925	0·33	6·32	12·71	34·3	41·1	0·51	2·70	98·0
5	950	0·57	6·11	12·49	32·9	39·7	0·42	3·20	95·4
Al spinel—synthetic Mg-annite gneiss (SMAG)									
3	900	0·54	0·65	49·68	24·9	13·3	0·47	10·12	99·7
3	925	1·47	0·41	52·32	19·9	11·4	0·54	14·45	100·5
5	925	0·32	0·43	53·25	26·1	9·8	0·36	9·54	99·8

[1]Values are averages of 3–4 analyses of different crystals. Typical relative uncertainties (2 S.D. of the mean values) are: SiO_2, ± 20%; TiO_2, ± 5%; Al_2O_3, ± 5%; FeO, ± 1%; MnO, ± 20%; MgO, ± 10%.
[2]Fe_2O_3 calculated by stoichiometry.

assemblages produced from more magnesian biotite-bearing sources [compare Patiño Douce & Beard (1995); see also Vielzeuf & Montel (1994)].

At $f(O_2) \leqslant$ QFM and $P \geqslant 5$ kbar (PC experiments) the melting reaction for SFAG and SMAG is of the form Bt + Pl + Qtz → Melt + Grt ± Opx + Oxides (Fig. 1, Table 4). This reaction is analogous to the pressure-sensitive melting reaction observed by Vielzeuf & Montel (1994, their reaction D) during fluid-absent melting of an aluminous metagreywacke. Alkali feldspar is also produced by the melting reaction of SFAG at $P = 15$ kbar, and minor amounts of alkali feldspar are also present in SMAG at 10 and 15 kbar (see discussion in previous section). Within the P and $f(O_2)$ conditions of PC experiments, consumption of plagioclase and production of garnet by the incongruent melting reaction increase with increasing pressure and with decreasing *mg*-number [Table 4, Fig. 1; see also Vielzeuf & Montel (1994) for pressure effect]. The effect of Fe/Mg ratio on the melting reaction causes the plagioclase stability field in SFAG at $P > 5$ kbar to be notably narrower than that in SMAG (Figs 1 and 3).

In each bulk composition the melt fraction produced at the biotite-out temperature (i.e. when all H_2O has been made available) changes slightly from 7 to 15 kbar (Figs 1 and 5, Table 4), owing to the

Table 10: Ilmenite compositions (wt %)[1]

P (kbar)	*T* (°C)	SiO_2	TiO_2	Al_2O_3	FeO	Fe_2O_3[2]	MnO	MgO	Total
Synthetic F-annite gneiss (SFAG)									
3	840	0·13	27·2	1·00	23·3	42·93	0·85	0·22	95·6
3	875	0·11	41·1	0·64	33·9	18·45	2·26	0·55	97·0
3	900	0·06	38·9	0·70	32·5	24·23	1·68	0·48	98·6
3	925	0·12	25·4	1·35	21·7	48·41	0·76	0·29	98·0
5	840	0·10	33·3	0·79	28·5	32·13	1·29	0·17	96·3
5	875	0·10	39·0	0·66	32·6	22·43	1·81	0·40	97·0
5	900	0·07	40·3	0·58	33·4	20·93	1·88	0·54	97·7
5	925	0·05	38·2	0·64	31·8	24·59	1·76	0·49	97·6
7	810	0·09	49·9	0·04	42·5	1·54	2·47	0·00	96·5
7	850	0·15	46·8	0·18	42·1	6·31	0·13	0·02	95·7
7	875	0·16	47·0	0·14	42·1	6·13	0·30	0·04	95·9
7	900	0·34	46·9	0·24	41·1	7·55	1·10	0·19	97·4
10	810	0·11	49·5	0·04	43·3	3·08	1·28	0·02	97·2
10	850	0·10	46·7	0·17	41·9	6·00	0·14	0·05	95·1
10	900	0·10	46·6	0·15	41·7	7·86	0·17	0·10	96·7
10	925	0·12	47·5	0·19	42·0	5·60	0·52	0·18	96·1
10	950	0·18	45·6	0·22	40·7	9·65	0·30	0·10	96·7
15	900	0·10	48·5	0·18	43·3	5·98	0·24	0·11	98·4
15	950	0·13	47·8	0·17	42·4	5·80	0·35	0·22	96·8
Synthetic Mg-annite gneiss (SMAG)									
3	840	0·18	22·1	1·63	17·4	52·24	0·33	1·30	95·2
3	875	0·15	35·5	0·94	28·0	31·72	0·40	2·10	98·7
3	900	0·14	29·4	1·33	23·0	42·50	0·31	1·82	98·5
3	925	0·16	22·9	1·85	16·8	51·74	0·24	2·11	95·8
5	840	0·25	27·5	1·31	22·4	43·50	0·53	1·17	96·6
5	850	0·18	47·3	0·23	40·3	7·57	0·14	1·30	97·1
5	875	0·12	28·5	1·38	23·1	42·99	0·19	1·37	97·6
5	900	0·17	30·1	1·45	24·2	40·31	0·25	1·60	98·1
5	925	0·24	30·9	1·37	24·9	38·47	0·25	1·65	97·8
7	810	0·13	49·7	0·15	43·5	3·51	0·36	0·56	98·0
7	850	0·04	49·7	0·22	42·1	3·12	0·15	1·40	96·7
7	875	0·24	49·0	0·21	41·7	3·71	0·25	1·31	96·4
7	900	0·13	50·2	0·25	41·3	2·50	0·61	1·87	96·8
10	810	0·24	48·1	0·17	42·0	5·71	0·10	0·80	97·1
10	850	0·14	49·6	0·18	42·1	3·22	0·12	1·42	96·7
10	900	0·16	49·8	0·18	41·6	4·46	0·11	1·79	98·1
10	925	0·12	49·7	0·25	40·2	3·47	0·18	2·51	96·5
10	950	0·15	49·9	0·26	40·9	3·61	0·21	2·25	97·3
15	900	0·33	51·3	0·32	42·5	4·20	0·12	2·18	101·0

[1]Values are averages of 3–4 analyses of different crystals. Typical relative uncertainties (2 S.D. of the mean values) are: SiO_2, ±100%; TiO_2, ±1%; Al_2O_3, ±40%; FeO, ±1%; MnO, ±10%; MgO, ±10%.
[2]Fe_2O_3 calculated by stoichiometry.

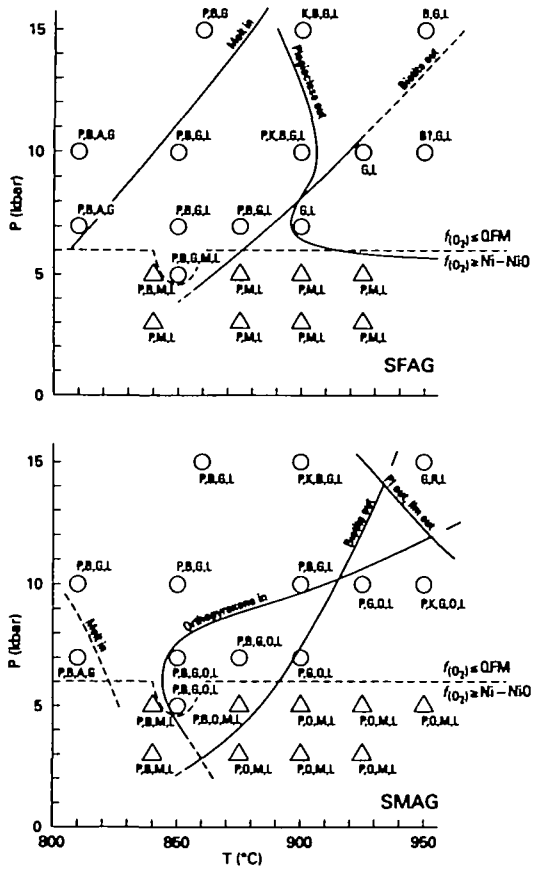

Fig. 3. Phase relations in the synthetic F-annite gneiss (SFAG, top) and in the synthetic Mg-annite gneiss (SMAG, bottom). Quartz and a Ti-oxide phase are always present. Other phases are as follows: B, biotite; P, plagioclase; K, alkali feldspar; O, orthopyroxene; G, garnet; M, magnetite ± Al-spinel; L, glass (quenched melt). The solidus of SFAG is approximated by a straight line within the T resolution of the experiments. Triangles show IHPV experiments and circles show PC experiments. The change in oxidation conditions corresponds to the change in experimental apparatus.

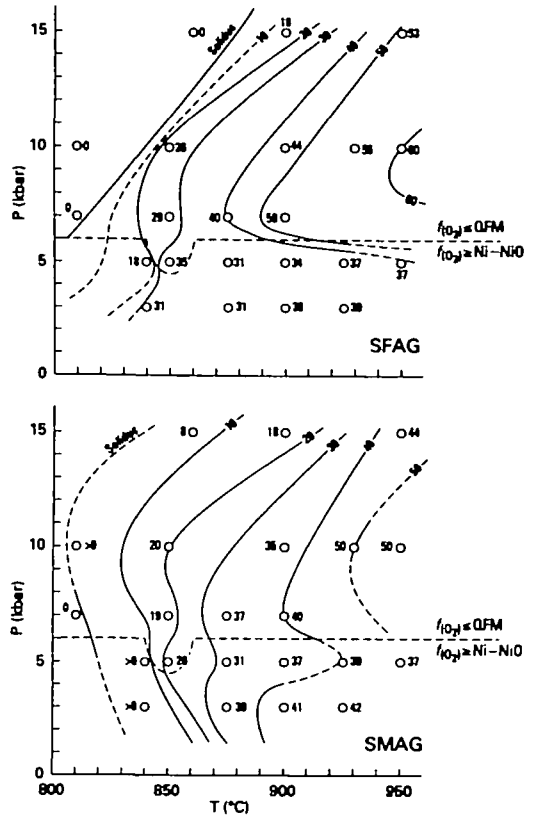

Fig. 4. Contours of constant melt fraction for SFAG (top) and for SMAG (bottom). (See also caption to Fig. 3.)

increased participation of plagioclase in the melting reaction with increasing P, which offsets the decrease in H_2O activity (at constant H_2O content) with increasing P. This effect is clearly demonstrated by Fig. 5, which shows that melt fraction at the biotite-out temperature increases with pressure as long as plagioclase is still present, and then decreases with increasing pressure beyond the plagioclase stability field. Thus, combination of the opposing effects of P on plagioclase stability and H_2O solubility dampens the influence of pressure on melt fraction [see also Patiño Douce & Beard (1995)].

Production of opx by the incongruent melting reaction is also a strong function of pressure and *mg*-number (see Table 4, Fig. 1). Opx is never stable in the more ferroan composition. It only crystallizes in SMAG on the low-P side of a phase boundary with

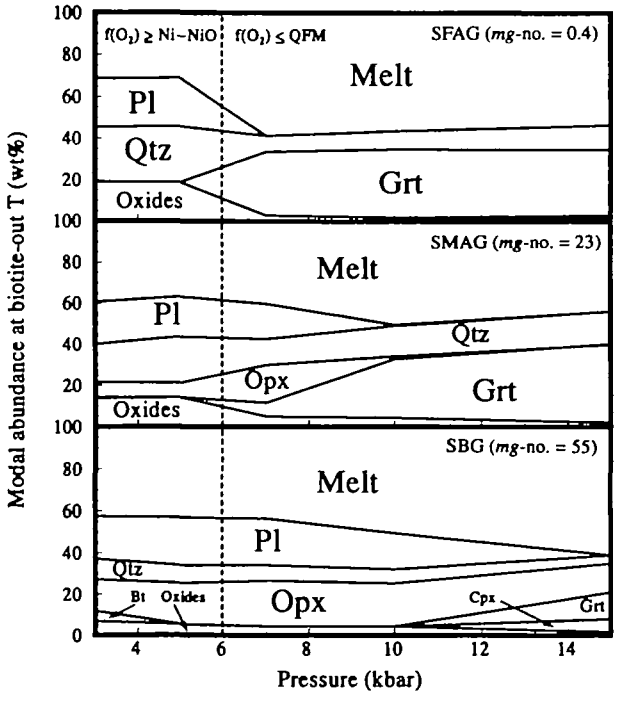

Fig. 5. Modal compositions at the biotite-out temperature as a function of pressure and oxygen fugacity (SBG data as in Fig. 2).

flat dP/dT slope (Fig. 3), and its modal abundance decreases strongly with increasing P (Fig. 1).

The melting reaction in the more oxidized IHPV experiments [$f(O_2) \geqslant$ Ni–NiO, $P \leqslant 5$ kbar] is of the form Bt + Pl + Qtz → Melt + Mag + Ilm (Table 4), with crystallization of opx (in the SMAG composition only) beginning a few tens of degrees above the solidus (Fig. 3). Suppression of garnet by high $f(O_2)$ causes a decrease in the proportion of plagioclase consumed by the dehydration melting reaction, relative to the more reduced PC experiments (see Fig. 5; compare also overlapping PC and IHPV experiments at 5 kbar in Table 4). This contributes to the notable widening of the plagioclase stability field in SFAG at $P \leqslant 5$ kbar, compared with higher-pressure experiments (Figs 1 and 3). In both SFAG and SMAG, the melt fraction at the biotite-out temperature is lower at 5 kbar and $f(O_2) \geqslant$ Ni–NiO than at 7 kbar and $f(O_2) \leqslant$ QFM, and the difference in melt fraction is largely compensated by greater modal abundances of plagioclase and quartz in the lower-pressure and more oxidized experiments (Figs 1 and 5). The change in melting behavior is clearly linked to garnet stability and demonstrates the importance of incongruent garnet-producing reactions in augmenting melt fraction from plagioclase-rich protoliths.

Effect of Fe/Mg ratio on melting relations of metagreywackes

A comparison of the melting relations of SFAG and SMAG with those of the more magnesian SBG composition (Patiño Douce & Beard, 1995) further elucidates the effects of Fe/Mg ratio on the melting behavior of metagreywackes, because the differences among them arise only from their biotite compositions.

Isobaric phase relations at $P = 10$ kbar and $f(O_2) \leqslant$ QFM are shown in Fig. 6a. Orthopyroxene

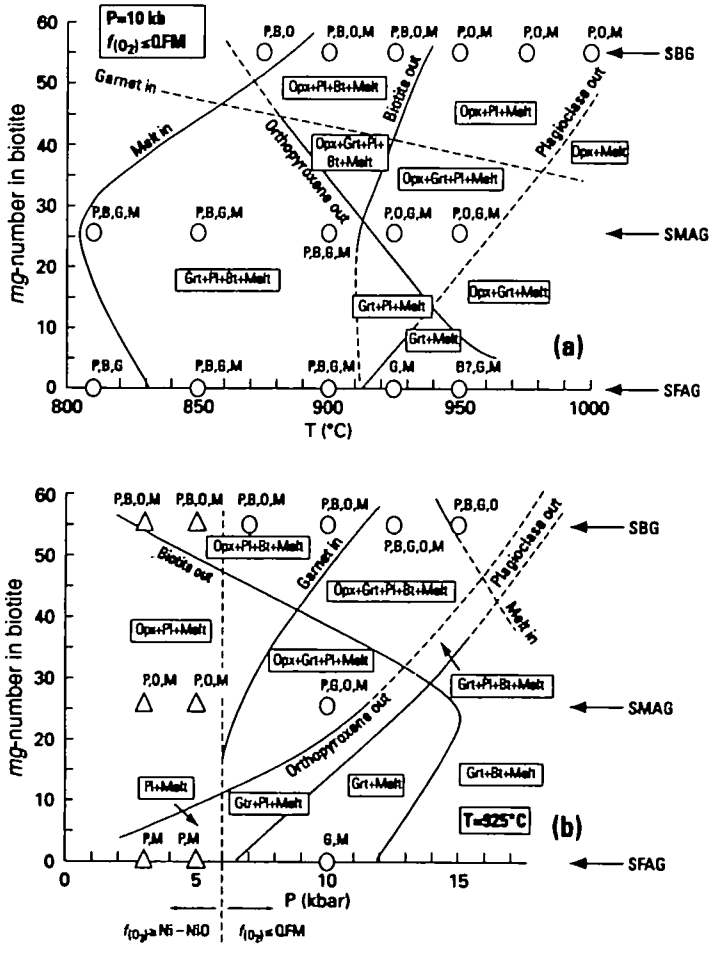

Fig. 6. (a) Isobaric phase relations [$P = 10$ kbar, $f(O_2) \leqslant$ QFM] as a function of mg-number and temperature. (b) Isothermal phase relations ($T = 925$°C) as a function of mg-number, pressure and $f(O_2)$. SBG data (mg-number 55) as in Fig. 2.

crystallizes on the high-T and high-*mg*-number side of its isobaric phase boundary, whereas plagioclase disappears on the high-T and low-*mg*-number side of the isobaric plagioclase-out boundary. At constant P, both the solidus and the biotite-out boundary have positive d(*mg*-number)/dT slopes between *mg*-numbers 23 and 55. At lower *mg*-number the slopes of both of these phase boundaries become negative. This inflection is almost certainly a consequence of the high F content of the more ferroan composition used in this study, and it is not likely to persist in F-free annitic compositions.

Isothermal phase relations at $T = 925$°C are shown in Fig. 6b. Orthopyroxene and plagioclase are stable on the low-P, high-*mg*-number side of their isothermal phase boundaries, whereas the opposite relations are true for garnet. The effect of the high F content of SFAG is again evident in the inflection of the biotite-out boundary, from negative d(*mg*-number)/dP slope at *mg*-number $\geqslant 23$, to positive at *mg*-number < 23.

In the experiments of Vielzeuf & Montel (1994) with an aluminous metagreywacke of *mg*-number 44, the garnet-in phase boundary at 925°C is located at $P = 7$–8 kbar. This pressure is ~ 2 kbar lower than that predicted from our experimental results for a protolith of the same *mg*-number (see Fig. 6b). Patiño Douce (1992) showed that the stability of garnet is also strongly affected by the activities of Al_2O_3 in the melt and of anorthite in plagioclase. For the ranges of pressure (≈ 7–10 kbar) and *mg*-number (≈ 25–50) encompassing the differences between our results and those of Vielzeuf & Montel (1994), garnet stability is a strong function of Al_2O_3 activity and a weak function of anorthite activity (Patiño Douce, 1992, figs 5 and 6). It is thus likely that garnet crystallization in the experiments of Vielzeuf & Montel (1994) at a slightly lower P than we would predict from our experiments is caused by the more aluminous composition of their starting material compared with SFAG, SMAG and SBG. The two sets of experiments are therefore not inconsistent.

The effects of *mg*-number on modal compositions are shown in Fig. 7, at 900°C (generally within the stability field of biotite), and 950°C (generally above the stability field of biotite). At high $f(O_2)$ (IHPV experiments at $P = 5$ kbar) silicate mafic phases (Opx ± Bt) are rapidly replaced by oxide phases (Mag ± Ilm) with decreasing *mg*-number. In con-

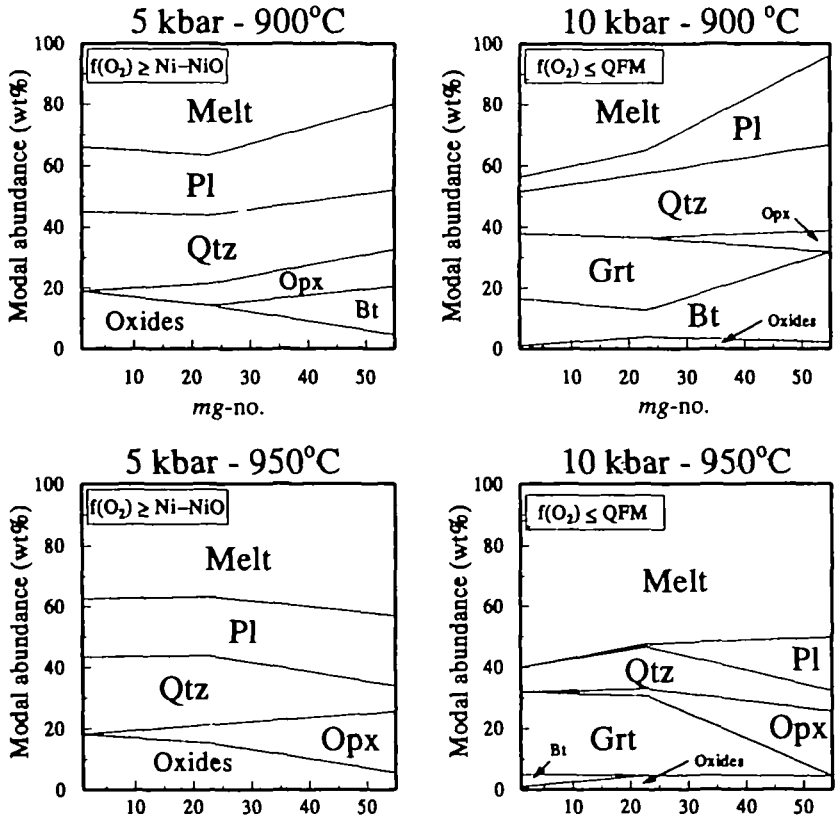

Fig. 7. Isobaric and isothermal modal compositions as a function of *mg*-number. SBG data (*mg*-number 55) as in Fig. 2.

trast, plagioclase abundance (especially once biotite stability has been exceeded) remains nearly constant with respect to *mg*-number, reflecting the fact that garnet is never stable at these P and $f(O_2)$ conditions. At more reducing conditions (PC experiments at $P = 10$ kbar) the modal proportion of oxide phases (ilmenite) is not very sensitive to *mg*-number and is always low ($\leqslant 4$ wt %). Decreasing *mg*-number at these conditions favors garnet crystallization. The assemblage Pl + Opx ± Bio is progressively replaced by the assemblage Grt + melt with decreasing *mg*-number (the increase in the modal abundance of biotite in SFAG at *mg*-number < 23 reflects the stabilizing effect of F). Comparison of the experiments at 5 kbar with those at 10 kbar (Fig. 7) demonstrates that garnet crystallization during dehydration melting enhances melt production with increasing pressure. A possible interpretation of this behavior (see Vielzeuf & Montel, 1994) is that garnet + melt are on the high-P side of the reaction Bt + Pl + Qtz → Grt + Melt. We believe, however, that this description is not complete, and that the important effect of Na in depressing the melting point of felsic melts (e.g. Tuttle & Bowen, 1958; Thompson & Algor, 1977) is to a large extent responsible for the observed increase in melt fraction (Fig. 7). Incongruent breakdown of plagioclase to grossular component in garnet increases the activity of albite, making more of this limiting component available for melting [see also discussion of melt compositions, below, and Patiño Douce & Johnston (1991)].

Melt compositions

Melts generated from both Fe-rich starting materials are silica rich, but melts generated from SMAG are always richer in SiO_2, generally in the range 73–77 wt % SiO_2, compared with melts generated from SFAG, which generally contain 70–73 wt % SiO_2 (Table 3). All the melts are granitic on the basis of the normative Ab–Or–An classification of Barker (1979), and peraluminous. Estimated H_2O contents are commonly less than 5 wt %, so that all the melts are strongly H_2O undersaturated.

Comparison of the melts derived from the two Fe-rich starting materials with those derived from the more magnesian SBG composition (Patiño Douce & Beard, 1995) demonstrates how different residual assemblages affect the major element compositions of granitic melts. In PC experiments [$P \geqslant 5$ kbar, $f(O_2) \leqslant$ QFM] garnet is the predominant mafic residual phase in SFAG and SMAG, but it is only present in SBG at $P \geqslant 12{\cdot}5$ kbar and in proportions subordinate to Opx ± Cpx (see Patiño Douce & Beard, 1995). Melts formed in equilibrium with

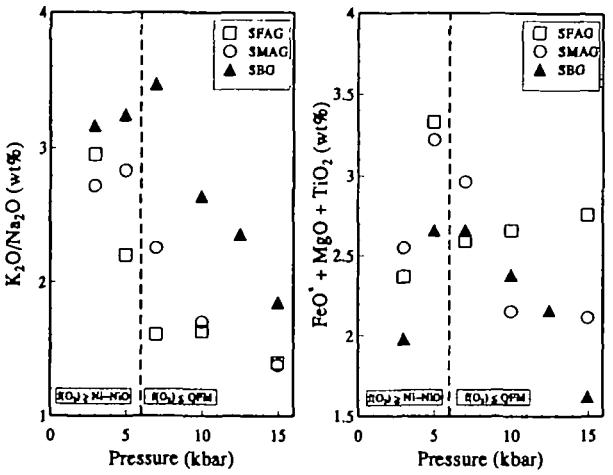

Fig. 8. Effects of pressure and $f(O_2)$ on K_2O/Na_2O ratios and $FeO^* + MgO + TiO_2$ contents of melts, interpolated at a constant melt fraction of 40%. SBG data as in Fig. 2.

garnet-rich residues, from the more ferroan starting materials, are more sodic and less calcic than melts formed at similar P–T–$f(O_2)$ conditions from the more magnesian SBG protolith, in the presence of little or no residual garnet (Fig. 8a). Melts derived from SBG show uniform drops in K_2O/Na_2O ratio and total $FeO + MgO + TiO_2$ contents with increasing pressure from 7 to 15 kbar (Fig. 8), as garnet (+ Cpx at $P = 15$ kbar) progressively joins the residual assemblage. Among SMAG melts, the K_2O/Na_2O ratio and $FeO + MgO + TiO_2$ content drop sharply from 5 to 10 kbar, as garnet replaces orthopyroxene (compare Figs 1 and 8). Among SFAG melts, where orthopyroxene is never stable and garnet is the only residual silicate mafic phase, both the K_2O/Na_2O ratio and the $FeO + MgO + TiO_2$ content remain nearly constant from 7 to 15 kbar (Fig. 8).

Removal of Ca from melts at $P \geqslant 5$ kbar (Table 3) is caused by garnet crystallization, which consumes the anorthite component of plagioclase to form grossular. As anorthite is consumed by this garnet-forming reaction the activity of albite increases, causing the melts to become more sodic (Fig. 8a). Garnet crystallization, however, also consumes Al_2O_3 in excess of that combined with grossular, to form almandine, pyrope and spessartine components. As a consequence, melts formed in equilibrium with garnet-rich residues in SFAG and SMAG are less peraluminous than SBG melts, equilibrated with residual assemblages dominated by pyroxene + plagioclase. This is shown by a comparison of their alumina saturation indices [ASI = molar $Al_2O_3/(CaO + Na_2O + K_2O)$, Fig. 9].

In contrast to PC experiments, at the conditions of

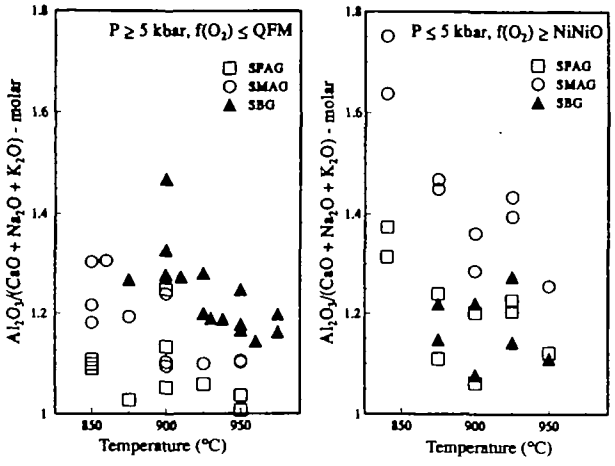

Fig. 9. ASI values [molar $Al_2O_3/(CaO + Na_2O + K_2O)$] as a function of temperature, for PC experiments (left), and IHPV experiments (right). SBG data as in Fig. 2.

IHPV experiments ($P \leqslant 5$ kbar, $f(O_2) \geqslant$ Ni–NiO) garnet is not stable in any of the three bulk compositions. In this case there is greater overlap in the Ab–An–Or contents of melts derived from SFAG, SMAG and SBG than among PC experiments, although SBG melts are always the most potassic (Fig. 8a). In the absence of residual garnet there also is greater overlap in the ASI values (Fig. 9) of melts derived from the three starting materials.

The total content of $FeO + MgO + TiO_2$ at constant melt fraction (Fig. 8b) tends to be lower in SBG melts than in the more Fe-rich SMAG and SFAG melts in both PC and IHPV experiments (the same relationship is observed if melt compositions are plotted in molar concentrations). The differences among the three bulk compositions are not uniform nor consistent, because the saturating ferromagnesian assemblages vary. However, the fact that SBG melts tend to be the most felsic among the three bulk compositions is consistent with MgO having a lower solubility than FeO in felsic melts.

DISCUSSION AND GEOLOGICAL APPLICATIONS

Melt compositions and melt fractions

Fluid-absent melting of Fe-rich metagreywackes yields peraluminous granitic melts that are similar in many respects to those that were obtained from more magnesian (and in some cases more aluminous) biotite-rich source materials by Le Breton & Thompson (1988), Vielzeuf & Holloway (1988), Patiño Douce & Johnston (1991), Skjerlie & Johnston (1993) and Patiño Douce & Beard (1995). However, our new results demonstrate that garnet-forming reactions have important effects on the Na/K ratio, Ca content and alumina saturation of crustal melts. These effects are particularly important during melting of non-peraluminous (or weakly peraluminous) source materials. In aluminosilicate-bearing metapelitic rocks, an aluminous ferromagnesian phase (garnet, cordierite, spinel) is invariably formed by incongruent dehydration melting reactions (e.g. Thompson, 1982; Vielzeuf & Holloway, 1988; Patiño Douce & Johnston, 1991). In contrast, crystallization of garnet during dehydration melting of less aluminous metagreywackes and tonalitic gneisses (orthogneisses) requires incongruent breakdown of anorthite to supply the necessary Al. This reaction liberates albite, causing increases in the melt fraction and in the Na_2O/K_2O ratio of the melts, compared with fluid-absent melting of biotite + plagioclase + quartz outside of the stability field of garnet. Crystallization of residual garnet during fluid-absent melting of subaluminous gneisses also drives the melts towards compositions that are less calcic and less peraluminous than those of melts formed from the same protoliths at conditions at which garnet is not stable. Our results also show that, at constant P, T, $f(H_2O)$ and $f(O_2)$, granitic melts tend to become more leucocratic as the Mg/Fe ratio of the source material increases.

Stabilization of residual garnet at the expense of plagioclase also has important effects on the trace element compositions of the coexisting melts. Melts formed in equilibrium with garnet-rich and plagioclase-free residues will be depleted in heavy rare-earth elements (HREE) but will not show negative Eu anomalies. These melts will also be enriched in Sr compared with melts formed in the presence of residual plagioclase. Such trace element signatures are found in many granitoid intrusions associated with regional metamorphic belts (e.g. Barbey *et al.*, 1990; Percival, 1991; Li *et al.*, 1991; Skjerlie, 1992; Barbero & Villaseca, 1992; Norman *et al.*, 1992). Garnet-rich and plagioclase-free residues can be generated over a wide range of crustal pressures, during melting of relatively Fe-rich, but not necessarily Al-rich, metasediments (compare Figs 1 and 5). In those cases in which the trace element compositions of relatively unfractionated silicic magmas suggest a garnet-rich and plagioclase-poor residue (HREE depletion, no Eu anomaly, high Sr content), it is possible to combine major and trace element compositions to better constrain the depth of melting. The *mg*-number of the garnet-rich residue can be estimated on the basis of Fe/Mg partitioning between garnet and melt (Ellis, 1986; Patiño Douce,

1996). This information, in turn, provides a lower (shallower) bound for the pressure of melting, as discussed in the following section.

Fluid-absent melting of SFAG also provides information about the effects of F-rich sources on the compositions of crustal melts. These results agree with those of Dooley & Patiño Douce (1996), who studied fluid-absent melting of the assemblage F-rich phlogopite + quartz + rutile. Both the Fe and the Mg end-members generate peraluminous, F-rich and felsic melts. We therefore argue that melting of halogen-enriched quartzofeldspathic gneisses is not a likely mechanism for the generation of metaluminous to peralkaline 'A-type' granites (e.g. Collins *et al.*, 1982; Whalen *et al.*, 1987). Rather, the peraluminous and F-rich melts (1·5–3 wt % F) formed by vapor-absent melting of SFAG [as well as the magnesian granitic melts obtained by Dooley & Patiño Douce (1996)] are similar to topaz rhyolites from the western USA (Christiansen *et al.*, 1983) and from Mongolia (ongonites; Kovalenko *et al.*, 1971). We suggest that these unusual volcanic rocks, and perhaps the strongly peraluminous macusanites (e.g. Pichavant & Montel, 1988) as well, are the most plausible candidates for natural melts of halogen-enriched crustal sources.

Garnet stability as a function of P, $f(O_2)$ and bulk composition

Our experiments constrain the effects of pressure, $f(O_2)$ and Fe/Mg ratio on garnet stability, for protoliths containing plagioclase of constant composition [An_{38}; see also Patiño Douce (1992)]. Given the important implications of residual garnet, it is desirable to construct a generalized description of how the interplay among these variables determines garnet stability. Such description is presented in Fig. 10, which shows isothermal phase relations projected onto the $f(O_2)$–pressure plane, at $T = 900°C$. The diagrams show the position of the garnet oxidation reaction

$$2Fe_3Al_2Si_3O_{12} + Ca_3Al_2Si_3O_{12} + O_2 \rightleftharpoons 2Fe_3O_4 + 3CaAl_2Si_2O_8 + 3SiO_2$$

for the three bulk compositions, SFAG, SMAG and SBG (see also Patiño Douce & Beard, 1995). This reaction produces magnetite, plagioclase and quartz, which is a common phase assemblage in IHPV experiments. The garnet oxidation reactions in Fig. 10 were calculated using garnet and plagioclase compositions observed in the experimental products

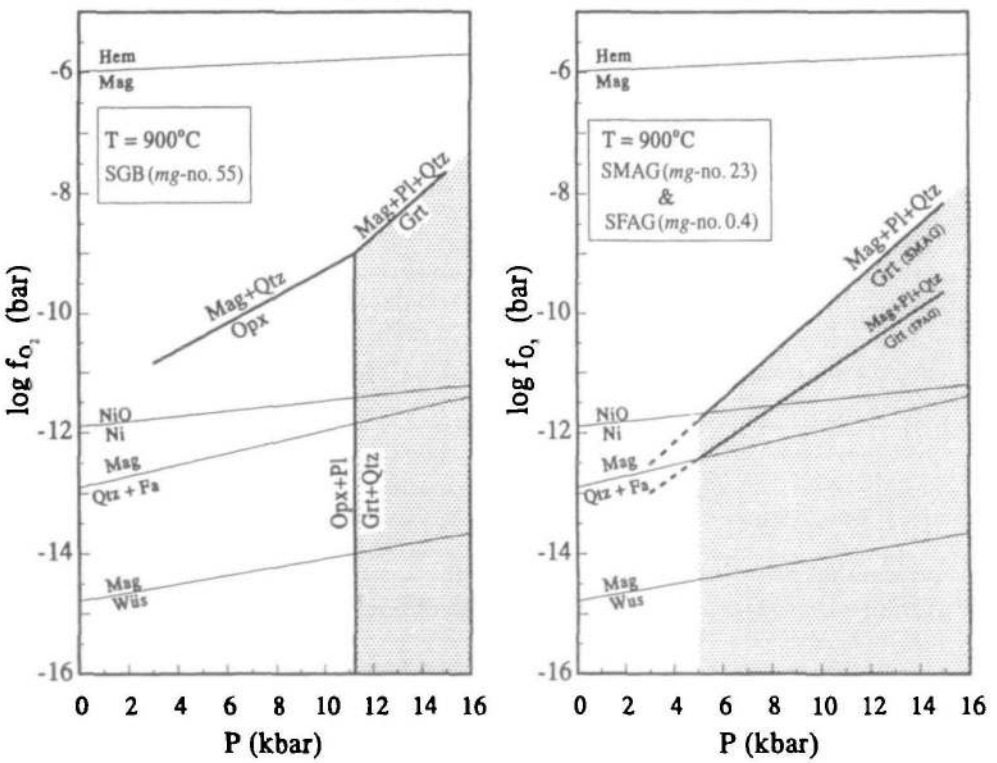

Fig. 10. Isothermal garnet stability fields (shaded) as a function of pressure, oxygen fugacity and *mg*-number of the starting material. SBG data as in Fig. 2. (See text for details on calculated phase boundaries.)

at each pressure studied and at temperatures of, or close to, 900°C. The solution models of Berman (1990) and Fuhrman & Lindsley (1988) were used for garnet and plagioclase, respectively, magnetite was assumed to be end-member Fe_3O_4, and all standard state thermodynamic properties were taken from Berman (1988). The calculated reactions are independent of $f(O_2)$ values estimated in the experimental products, because oxygen fugacity was the dependent variable in the calculations. The calculated reactions, however, correctly predict the phase relations observed in the experimental products. For example, at 5 kbar the diagrams indicate that garnet should be stable in PC experiments [$f(O_2) \leqslant$ QFM] with both SFAG and SMAG, and that it should not be stable in IHPV experiments [$f(O_2) \geqslant$ Ni–NiO] at the same pressure (compare Table 2).

In addition to the garnet oxidation reaction, for the more magnesian composition SBG the diagram in Fig. 10 shows: (1) the approximate position of the oxygen-independent breakdown of garnet + quartz to orthopyroxene + plagioclase [as inferred from the phase relations determined by Patiño Douce & Beard (1995)], and (2) the approximate position of the orthopyroxene–magnetite–quartz oxidation reaction, constrained by phase assemblages in IHPV experiments (see Patiño Douce & Beard, 1995) and by the intersection between the two garnet breakdown reactions.

The shaded regions in Fig. 10 indicate the ranges of P–$f(O_2)$ conditions within which garnet is stable. Incongruent breakdown of plagioclase within these regions leads to increased melting and to changes in melt composition, such as higher Na_2O and Sr contents. Crustal anatexis is likely to take place in the mid to lower continental crust, and it is certainly not possible to make a general statement about the oxidation conditions prevalent in that segment of the lithosphere. A review of the literature suggests that a large proportion of high-grade metamorphic terranes, both graphite bearing and graphite free, equilibrated under fairly reduced conditions, commonly between the QFM and magnetite–wüstite buffers (e.g. Tracy, 1978; Grew, 1981; Lamb & Valley, 1984; Powers & Bohlen, 1985; Srikantappa *et al.*, 1985; Battacharya & Sen, 1986; Valley *et al.*, 1990). Under such conditions, oxygen fugacity is not the variable that limits garnet stability, even in Fe-rich bulk compositions (Fig. 10). Crystallization of garnet at the expense of plagioclase is controlled in this case by the pressure-sensitive and $f(O_2)$-independent reaction orthopyroxene + plagioclase → garnet + quartz (see Fig. 10). The depth at which this reaction takes place is controlled by the Fe/Mg ratio and plagioclase composition of the source material. In a protolith with mg-number = 23 (SMAG) garnet crystallization would take place even during fairly shallow melting ($P \leqslant 5$ kbar). Thus, melting of Fe-rich metasediments in reducing environments (e.g. melting of sulfide-rich schists) can generate large melt fractions over a wide range of crustal pressures. In contrast, in a protolith with mg-number = 57 (SBG) garnet would only crystallize if melting took place deep within thick continental crust ($P > 10$ kbar). The garnet–quartz–orthopyroxene–plagioclase reaction shifts to higher pressure with decreasing anorthite content in plagioclase, but the magnitude of this displacement is not constant with respect to pressure or Fe/Mg ratio, as shown by the phase diagrams of Patiño Douce (1992, figs 4–7). The effect of plagioclase composition is negligible in Fe-rich bulk compositions and at low pressure (≈ 5 kbar), so that termination of garnet stability in favor of orthopyroxene during shallow crustal melting would be unlikely in protoliths analogous to SFAG or SMAG but with more sodic plagioclase. In contrast, in a protolith such as SBG the presence of more sodic plagioclase could shift the garnet-in boundary to pressures in excess of 15 kbar.

Some high-grade terranes, however, record $f(O_2)$ conditions that are more oxidized than QFM, in the neighborhood of the Ni–NiO buffer (e.g. Riciputi *et al.*, 1990; Sengupta *et al.*, 1991). In this case low-P fluid-absent melting of Fe-rich protoliths could be notably curtailed by the stabilization of the assemblage plagioclase + magnetite (Fig. 10), but there would be no change in the melting behavior of Mg-rich protoliths, compared with more reducing conditions. In fact, for a protolith such as SBG, oxidation of garnet would not limit melt production unless the prevailing oxygen fugacity was 6–7 orders of magnitude higher than the QFM buffer. Such highly oxidized conditions are probably rare in the deep crust.

Implications for crustal magmatism

Because both Na_2O and H_2O are essential components of low-temperature felsic melts (e.g. Tuttle & Bowen, 1958; Thompson & Algor, 1977; Patiño Douce & Johnston, 1991), crystallization of garnet during dehydration melting of subaluminous metamorphic rocks plays a crucial role in preserving (or even increasing) melt productivity with increasing pressure (e.g. Figs 5 and 10). This may help to explain why orogenic thickening of the continental crust leads to conditions that are particularly favorable for the generation of felsic magmas. On the one hand, tectonic crustal thickening favors attainment of melting temperatures, as a con-

sequence of thermal blanketing (e.g. England & Thompson, 1986; Patiño Douce *et al.*, 1990), or density entrapment of basaltic melts (e.g. Bergantz & Dawes, 1994), or thermal erosion of the subcrustal lithosphere (e.g. Houseman *et al.*, 1981; Loosveld & Etheridge, 1990; Sacks & Secor, 1990), or a combination of all of these processes. On the other hand, quartzofeldspathic metamorphic rocks will remain fertile sources for felsic magmas at high pressures ($\sim$ 10–15 kbar), owing to incongruent breakdown of plagioclase within the stability field of garnet. This is true whether or not infiltration of externally derived aqueous fluids takes place. The large granitoid batholiths that are often formed at the cores of orogenic belts, and that often show strongly fractionated (HREE-depleted) REE patterns, may thus be the products of the convergence, in thickened continental crust, of favorable thermal and phase equilibrium conditions for crustal anatexis.

ACKNOWLEDGEMENTS

We thank Todd Dunn, Bob Tracy and Donna Whitney for their very constructive reviews of this manuscript, and Sorena Sorensen for her editorial help. We are indebted to Gary Lofgren for making it possible to perform IHPV experiments at Johnson Space Center. This work was supported by NSF Grants EAR-9118418 and EAR-9316304 to A.E.P.D. and EAR-9120035 to J.S.B. The microprobe at the University of Georgia was acquired with NSF Grant EAR-8816748 and a matching grant from the University of Georgia Research Foundation.

REFERENCES

Barbero, L. & Villaseca, C., 1992. The Layos granite, Hercynian complex of Toledo (Spain): an example of parautochthonous restite-rich granite in a granulite area. *Transactions of the Royal Society of Edinburgh: Earth Sciences* **83**, 127–138.

Barbey, P., Macaudiere, J. & Nzenti, P., 1990. High-pressure dehydration melting of metapelites: evidence from the migmatites of Yaoundé (Cameroon). *Journal of Petrology* **31**, 401–427.

Barker, F., 1979. Trondhjemite: definition, environment and hypotheses of origin. In: Barker, F. (ed.) *Trondhjemites, Dacites, and Related Rocks. Developments in Petrology, 6.* Amsterdam: Elsevier, pp. 1–12.

Battacharya, A. & Sen, S. K., 1986. Granulite metamorphism, fluid buffering and dehydration-melting in the Madras charnockites and metapelites. *Journal of Petrology* **27**, 1119–1141.

Bergantz, G. W. & Dawes, R., 1994. Aspects of magma generation and ascent in continental lithosphere. In: Ryan, M.P. (ed.) *Magmatic Systems*. New York: Academic Press, pp. 291–317.

Berman, R. G., 1988. Internally-consistent thermodynamic data for stoichiometric minerals in the system Na_2O–K_2O–CaO–MgO–FeO–Fe_2O_3–Al_2O_3–SiO_2–TiO_2–H_2O–CO_2. *Journal of Petrology* **29**, 445–522.

Berman, R. G., 1990. Mixing properties of Ca–Mg–Fe–Mn garnets. *American Mineralogist* **75**, 328–344.

Bohlen, S., Essene, E. J. & Boettcher, A. L., 1980. Re-investigation and application of olivine–quartz–orthopyroxene barometry. *Earth and Planetary Science Letters* **47**, 11–20.

Burnham, C. W., 1979. Magmas and hydrothermal fluids. In: Barnes, H. L. (ed.) *Geochemistry of Hydrothermal Ore Deposits*, 2nd edn. New York: Wiley Interscience, pp. 71–136.

Carrington, D. P. & Watt, G. R., 1995. A geochemical and experimental study of the role of K-feldspar during water-undersaturated melting of metapelites. *Chemical Geology* **122**, 59–76.

Christiansen, E. H., Burt, D. M., Sheridan, M. F. & Wilson, R. T., 1983. The petrogenesis of topaz rhyolites from the Western United States. *Contributions to Mineralogy and Petrology* **83**, 16–30.

Clemens, J. D. & Vielzeuf, D., 1987. Constraints on melting and magma production in the crust. *Earth and Planetary Science Letters* **86**, 287–306.

Collins, W. J., Beams, S. D., White, A. J. R. & Chappell, B. W., 1982. Nature and origin of A-type granites with particular reference to southeastern Australia. *Contributions to Mineralogy and Petrology* **80**, 189–200.

Dooley, D. F. & Patiño Douce, A. E., 1996. Vapor-absent melting of F- and Ti-rich phlogopite + quartz; effects on phlogopite stability and melt compositions. *American Mineralogist* **81**, 202–212.

Dymek, R. F., 1983. Titanium, aluminum and interlayer cation substitutions in biotite from high-grade gneisses, West Greenland. *American Mineralogist* **68**, 880–899.

Ellis, D. J., 1986. Garnet–liquid Fe^{2+}–Mg equilibria and implications for the beginning of melting in the crust and subduction zones. *American Journal of Science* **286**, 765–791.

England, P. C. & Thompson, A. B., 1986. Some thermal and tectonic models for crustal melting in continental collision zones. In: Coward, M.P. & Ries, A.C. (eds) *Collision Tectonics. Geological Society Special Publication* **19**, 83–94.

Fuhrman, M. L. & Lindsley, D. H., 1988. Ternary-feldspar modeling and thermometry. *American Mineralogist* **73**, 201–215.

Gardien, V., Thompson, A. B., Grujic, D. & Ulmer, P., 1995. Experimental melting of biotite + plagioclase + quartz ± muscovite assemblages and implications for crustal melting. *Journal of Geophysical Research* **100**, 15581–15591.

Ghiorso, M. S., 1990. Thermodynamic properties of hematite–ilmenite–geikielite solid solutions. *Contributions to Mineralogy and Petrology* **104**, 645–667.

Grew, E. S., 1981. Granulite-facies metamorphism at Molodezhnaya Station, East Antarctica. *Journal of Petrology* **22**, 297–336.

Houseman, G. A., McKenzie, D. P. & Molnar, P., 1981. Convective instability of a thickened boundary layer and its relevance for the thermal evolution of continental convergent belts. *Journal of Geophysical Research* **86**, 6115–6132.

Kovalenko, V. L., Kuz'min, M. I., Antipin, V. S. & Petrov, L. L., 1971. Topaz-bearing quartz keratophyre (ongonite), a new variety of subvolcanic igneous vein rock. *Doklady Akademii Nauk SSSR* **199**, 132–135.

Kretz, R., 1983. Symbols for rock-forming minerals. *American Mineralogist* **68**, 277–279.

Lamb, W. & Valley, J. W., 1984. Metamorphism of reduced granulites in low-CO_2 vapour-free environment. *Nature* **312**, 56–58.

Lambert, I. B. & Wyllie, P. J., 1972. Melting of gabbro (quartz eclogite) with excess water to 35 kilobars, with geological applications. *Journal of Geology* **80**, 693–708.

Le Breton, N. & Thompson, A. B., 1988. Fluid-absent (dehydration) melting of biotite in metapelites in the early stages of crustal anatexis. *Contributions to Mineralogy and Petrology* **99**, 226–237.

Li, H., Schwarcz, H. P. & Shaw, D. M., 1991. Deep crustal oxygen isotope variations: the Wawa–Kapuskasing crustal transect, Ontario. *Contributions to Mineralogy and Petrology* **107**, 448–458.

Loosveld, R. J. H. & Etheridge, M. A., 1990. A model for low-pressure facies metamorphism during crustal thickening. *Journal of Metamorphic Geology* **8**, 257–267.

Munoz, J. L., 1984. F–OH and Cl–OH exchange in micas with applications to hydrothermal ore deposits. *Reviews in Mineralogy* **13**, 469–494.

Norman, M. D., Leeman, W. P. & Mertzman, S. A., 1992. Granites and rhyolites from the northwestern U.S.A.: temporal variations in magmatic processes and relations to tectonic setting. *Transactions of the Royal Society of Edinburgh: Earth Sciences* **83**, 71–81.

Patiño Douce, A. E., 1992. Calculated relationships between activity of alumina and phase assemblages of silica-saturated igneous rocks: petrogenetic implications of magmatic cordierite, garnet and aluminosilicate. *Journal of Volcanology and Geothermal Research* **52**, 43–63.

Patiño Douce, A. E., 1993. Titanium substitution in biotite: an empirical model with applications to thermometry, O_2 and H_2O barometries, and consequences for biotite stability. *Chemical Geology* **108**, 133–162.

Patiño Douce, A. E., 1995. Experimental generation of hybrid silicic melts by reaction of high-Al basalt with metamorphic rocks. *Journal of Geophysical Research* **100**, 15623–15639.

Patiño Douce, A. E., 1996. Effects of pressure and H_2O content on the compositions of primary crustal melts. *Transactions of the Royal Society of Edinburgh: Earth Sciences*, in press.

Patiño Douce, A. E. & Beard, J. S., 1994. Water loss from hydrous melts during fluid-absent piston-cylinder experiments. *American Mineralogist* **79**, 585–588.

Patiño Douce, A. E. & Beard, J. S., 1995. Dehydration-melting of biotite gneiss and quartz amphibolite from 3 to 15 kbar. *Journal of Petrology* **36**, 707–738.

Patiño Douce, A. E. & Johnston, A. D., 1991. Phase equilibria and melt productivity in the pelitic system: implications for the origin of peraluminous granitoids and aluminous granulites. *Contributions to Mineralogy and Petrology* **107**, 202–218.

Patiño Douce, A. E., Humphreys, E. D. & Johnston, A. D., 1990. Anatexis and metamorphism in tectonically thickened continental crust exemplified by the Sevier hinterland, western North America. *Earth and Planetary Science Letters* **97**, 290–315.

Percival, J. A., 1991. Granulite-facies metamorphism and crustal magmatism in the Ashuanipi Complex, Quebec–Labrador, Canada. *Journal of Petrology* **32**, 1261–1297.

Peterson, J. W., Chacko, T. & Kuehner, S. M., 1991. The effects of fluorine on the vapor-absent melting of phlogopite + quartz: implications for deep-crustal processes. *American Mineralogist* **76**, 470–476.

Pichavant, M. & Montel, J. M., 1988. Petrogenesis of a two-mica ignimbrite suite: the Macusani volcanics, SE Perú. *Transactions of the Royal Society of Edinburgh: Earth Sciences* **79**, 197–207.

Powers, R. E. & Bohlen, S. R., 1985. The role of synmetamorphic igneous rocks in the metamorphism and partial melting of metasediments, Northwest Adirondacks. *Contributions to Mineralogy and Petrology* **90**, 401–409.

Ramberg, H., 1948. Titanic iron ore formed by dissociation of silicates in granulite facies. *Economic Geology* **43**, 553–570.

Riciputi, L. R., Valley, J. W. & McGregor, V. R., 1990. Conditions of Archean granulite metamorphism in the Godthab–Fiskenaesset region, southern West Greenland. *Journal of Metamorphic Geology* **8**, 171–190.

Robert, J. L., 1976. Titanium solubility in synthetic phlogopite solid solutions. *Chemical Geology* **17**, 213–227.

Rushmer, T., 1991. Partial melting of two amphibolites: contrasting experimental results under fluid absent conditions. *Contributions to Mineralogy and Petrology* **107**, 41–59.

Rutter, M. J. & Wyllie, P. J., 1988. Melting of vapour-absent tonalite at 10 kbar to simulate dehydration-melting in the deep crust. *Nature* **331**, 159–160.

Sack, R. O. & Ghiorso, M. S., 1989. Importance of considerations of mixing properties in establishing an internally consistent thermodynamic database: thermochemistry of minerals in the system Mg_2SiO_4–Fe_2SiO_4–SiO_2. *Contributions to Mineralogy and Petrology* **102**, 41–68.

Sacks, P. E. & Secor, Jr., D. T., 1990. Delamination of collisional orogens. *Geology* **18**, 999–1002.

Sengupta, P., Karmakar, S., Dasgupta, S. & Fukuoka, M., 1991. Petrology of spinel granulites from Araku, Eastern Ghats, India, and a petrogenetic grid for sapphirine-free rocks in the system FMAS. *Journal of Metamorphic Geology* **9**, 451–459.

Skjerlie, K. P., 1992. Petrogenesis and significance of late Caledonian granitoid magmatism in western Norway. *Contributions to Mineralogy and Petrology* **110**, 473–487.

Skjerlie, K. P. & Johnston, A. D., 1993. Fluid-absent melting behavior of an F-rich tonalitic gneiss at mid-crustal pressures: implications for the generation of anorogenic granites. *Journal of Petrology* **34**, 785–815.

Srikantappa, C., Raith, M. & Spiering, B., 1985. Progressive charnockitization of a leptynite–khondalite suite in southern Kerala, India—Evidence for formation of charnockites through decrease in fluid pressure? *Journal of the Geological Society of India* **26**, 849–872.

Thompson, A. B., 1982. Dehydration melting of pelitic rocks and the generation of H_2O-undersaturated granitic liquids. *American Journal of Science* **282**, 1567–1595.

Thompson, A. B., 1996. Fertility of crustal rocks during anatexis. *Transactions of the Royal Society of Edinburgh: Earth Sciences*, in press.

Thompson, A. B. & Algor, J. R., 1977. Model system for anatexis of pelitic rocks. I. Theory of melting reactions in the system $KAlO_2$–$NaAlO_2$–Al_2O_3–SiO_2–H_2O. *Contributions to Mineralogy and Petrology* **63**, 247–269.

Tracy, R. J., 1978. High grade metamorphic reactions and partial melting in pelitic schist, west-central Massachusetts. *American Journal of Science* **278**, 150–178.

Trønnes, R. G., Edgar, A. D. & Arima, M., 1985. A high pressure–high temperature study of TiO_2 solubility in Mg-rich phlogopite: implications to phlogopite chemistry. *Geochimica et Cosmochimica Acta* **49**, 2323–2329.

Tuttle, O. F. & Bowen, N. L., 1958. Origin of granite in the light of experimental studies in the system $KAlSi_3O_8$–$NaAlSi_3O_8$–SiO_2–H_2O. *Geological Society of America Memoir* **74**.

Valley, J. W., Bohlen, S. R., Essene, E. J. & Lamb, W., 1990. Metamorphism in the Adirondacks: II. The role of fluids. *Journal of Petrology* **31**, 555–596.

Vielzeuf, D. & Clemens, J. D., 1992. The fluid-absent melting of phlogopite + quartz: experiments and models. *American Mineralogist* **77**, 1206–1222.

Vielzeuf, D. & Holloway, J. R., 1988. Experimental determination of the fluid-absent melting relations in the pelitic system. Consequences for crustal differentiation. *Contributions to Mineralogy and Petrology* **98**, 257–276.

Vielzeuf, D. & Montel, J. M., 1994. Partial melting of metagreywackes. 1. Fluid-absent experiments and phase relationships. *Contributions to Mineralogy and Petrology* **117**, 375–393.

Whalen, J. B., Currie, K. L. & Chappell, B. W., 1987. A-type granites: geochemical characteristics, discrimination and petrogenesis. *Contributions to Mineralogy and Petrology* **95**, 407–419.

Wyllie, P. J. & Wolf, M. B., 1993. Amphibole dehydration-melting: sorting out the solidus. In: Prichard, H. M., Alabaster, T., Harris, N. B. W. & Neary, C. R. (eds) *Magmatic Processes and Plate Tectonics. Geological Society Special Publication* **76**, 405–416.

RECEIVED NOVEMBER 8, 1995
REVISED TYPESCRIPT ACCEPTED APRIL 12, 1996